RAPID DNA-BASED POINT-OF-CARE DIAGNOSTICS

by

ASHISH SURESH YERI

B.E Chemical Engineering, Visveswaraiah Technological University, 2006

Submitted to the Graduate Faculty of

Swanson School of Engineering in partial fulfillment

of the requirements for the degree of

Doctor of Philosophy

University of Pittsburgh

2011

UNIVERSITY OF PITTSBURGH

SWANSON SCHOOL OF ENGINEERING

This dissertation was presented

by

ASHISH SURESH YERI

It was defended on

November 23, 2011

and approved by

Mohammad Ataai, Ph.D.,Professor, Department of Chemical and Petroleum Engineering

Steven Little, Ph.D., Assistant Professor, Department of Chemical and Petroleum Engineering

Abhay Vats, M.D., Assistant Professor of Pediatrics, University of Pittsburgh School of Medicine

Dissertation Director: Di Gao, Ph.D., Associate Professor, Department of Chemical and Petroleum Engineering

RAPID DNA-BASED POINT-OF-CARE DIAGNOSTICS

Ashish Suresh Yeri, Ph.D.

University of Pittsburgh, 2011

DNA-based biosensors for detection of genetic mutations and infectious diseases have attracted a lot of attention recently owing to the large amount of genetic information available and the high specificity of these sensors due to the uniqueness of DNA sequences.

In the first part of my work, the viscoelastic properties of single-strand DNA are made use of to rapidly screen for disease causing mutations. Single strand DNA (ssDNA) films have viscoelastic properties which are dependent on their 3-D conformation in solution which in turn is dependent on their base sequence. The mutation of the *p53* gene which is responsible for almost half of all cancers was chosen as our case study. The appreciable differences in the viscoelastic properties between the *p53* wild type ssDNA film and the *p53* mutant R type ssDNA film were evaluated using a quartz crystal resonator showing that this method holds much promise to be used as a rapid DNA mutation screening technique.

In the second part of my work, we have made use of novel isothermal DNA amplification techniques to specifically amplify the target DNA which is then detected on lateral flow strips in a low cost manner. *Escherichia coli and Klebsiella pneumoniae* are responsible for a large number of infections including Urinary Tract Infection (UTI) and life threatening conditions such as neonatal meningitis and neonatal sepsis. A rapid and sensitive detection scheme has been developed for these bacteria by amplification of the DNA with Loop mediated isothermal amplification technique (LAMP) and its subsequent detection on lateral flow strips. Patient urine samples were screened for the presence of these two organisms and the LAMP-lateral flow detection scheme is comparable to the bacterial culture methods which is the current gold

standard. Furthermore, multiplexing the amplification and detection has been demonstrated successfully which shows great potential to be employed as a reliable point-of-care diagnostic tool in the clinical setting.

TABLE OF CONTENTS

LIST OF TABLES

LIST OF FIGURES

ACKNOWLEDGEMENTS

I would like to thank Dr. Lizeng Gao and Dr. Chandramohan Ishwad who have mentored and guided me at every step through the rigors of lab work. Without their able guidance and generosity, this work would not have been possible. I am grateful to Ashok Gurung and Nilesh Dhamne for their tremendous support and help with the LAMP-lateral flow project. I would like to thank Dr. Haim Bau's group at the University of Pennsylvania for the training I received for the preparation of lateral flow strips and Ally McManus for her assistance in the LAMP multiplex detection. I am grateful to all my lab members for their help and support and a special mention goes out to Jiamin Wu for his unabated assistance in the lab. I am indeed indebted to Dr. Di Gao and Dr. Abhay Vats, for being a constant source of inspiration and for the patience and faith shown in me. I am ever grateful to their incisive suggestions and remarkable foresight throughout the project.

I am ever obliged to Dr. H. S. Muralidhara and Dr. R. Kumar for their support and encouragement through my student life. And lastly, but most importantly, I am humbled by the support, love and affection shown to me by my family and friends who make living an absolute joy.

1.0 INTRODUCTION

Sensors which incorporate biomolecules such as cells, proteins/antibodies or DNA to sense the target analyte which may be another biomolecule, trace chemicals, etc. are termed biosensors. Typically these biomolecules are integrated to the transducer surface via physical adsorption or chemisorption. The interaction or binding between the target analyte and the biomolecule is sensed by the sensor which is converted into an analytical signal to be amplified or processed.

The greatest advantage offered by biosensors is their sensitivity and selectivity to the target analyte from a complex media. The selectivity is entirely due to the choice of the right biomolecule (the sensing element) which should have the highest affinity for the target analyte whereas the sensitivity is affected by the orientation of the biomolecules after immobilization onto the transducer surface and also the efficiency with which the transducer detects this interaction [1]. The former aspect is discussed in detail in chapter 3.2.

Biosensors which are based on the affinity between the target analyte to the biomolecule are termed affinity based biosensors where the target analyte binds irreversibly to the biomolecule as in the case of sensors which are based on antigen-antibody or hapten-antibody interaction. In catalytic biosensors, the concentration of the target analyte is related to the progress of a chemical reaction which is bio-catalyzed[2]. The glucose biosensor which accounts for 85% of the market [3]for biosensors is based on the enzyme glucose oxidase which oxidizes β-D Glucose to gluconic acid and hydrogen peroxide. The amount of glucose is sensed by measuring the amount of oxygen consumed, or by measuring the amount of hydrogen-peroxide formed or by measuring the electron flow resulting from the oxidation reaction[4].

The function of the transducer is to sense the physico-chemical change induced after the target binds to the biomolecule and to convert it into a measurable quantity. The commonly used transducers are optical transducers, thermometric transducers, piezoelectric transducers and electrochemical. Biosensors find uses in a plethora of fields such as in the medical field in the detection of pathogens, tumor markers, toxic metabolites, glucose monitoring, and routine analytical measurement of patient samples in point-of-care diagnostics. In the food industry, biosensors are used for the detection of bacteria in decaying food and to assess process quality. They are used in drug discovery and in the evaluation of biological activity of new compounds. Recently, they have been used in the detection of chemical weapons, drugs and narcotics.

DNA-based Biosensors

Biosensors which incorporate DNA molecules as the sensing element are termed as DNA biosensors. With the enormous success of the human genome project, a large amount of genetic data has been made available rapidly which holds great promise for detection of genetic diseases early on which could possibly prevent their occurrence by administering the right treatment. The uniqueness of the DNA sequences whether one is looking to detect point mutations in cancer research and therapy or for the detection of one among many bacterial/viral strains makes the use of DNA biosensors as specific as there can be at the moment. Furthermore, in many cases the isolation of the pathogenic micro-organisms is not necessary and the detection can be carried out with the contents from the dead cells. This provides a big advantage over cell culture methods which are tedious and time consuming. Therefore there is a need for design of simple, rapid, affordable DNA based biosensors which not only would help in decentralizing diagnostic testing, but would also be useful to be deployed in third world countries where sensitive, rapid and cheap diagnostics would be invaluable.

Currently most of the DNA biosensors are based on nucleic acid (NA) hybridization. Single strand DNA (ssDNA) hydrogen bond to other ssDNA strands according to the Watson-Crick pairing rules: Adenine with Thymine (forming two hydrogen bonds) and Cytosil with Guanine (forming three hydrogen bonds) which is termed as DNA-DNA hybridization. Typically a short single strand DNA (ssDNA) molecule (10-30 mers) is immobilized onto the surface of the transducing element and is allowed to bind to its complementary strand in solution. The most common transducing techniques employed to detect the hybridization are optical, electrochemical and piezoelectric and colorimetric.

1.1 OPTICAL TRANSDUCTION

Optical transduction makes use of optic-fiber cables where the excitation light of a particular wavelength from the source passes through the optic-fiber cable by a series of total internal reflections due to the difference in the refractive indices of the core of the optic-fiber and the cladding. Excitation light of a particular wavelength is passed through the optic-fiber which excites the fluorescent labeled biomolecule and the light emitted by the label passes through the same optic-fiber cable which is separated and detected by an optical detector. Typically, the ssDNA probe is attached to the optic-fiber at the distal end, [5,6]or on the outer surface of the core[7-9]. The hybridization of the complementary sequence to an immobilized ssDNA probe can be detected in one of two ways. After hybridization, double strand DNA (dsDNA) specific fluorescent dyes such as Ethidium bromide[8], PicoGreen[6] are allowed to bind to the dsDNA complex and the fluorescence can be detected by an optic fiber or fluorescently labeled complementary strands are allowed to bind to the immobilized ssDNA on the optic-fiber surface. Short ssDNA probes (16-20 mer) were used to detect fluorescent labeled DNA targets on the surface of an optic fiber cable[10]. The detection of hybridization of 16 mer fluorescent labeled ssDNA strands in solution to ssDNA probe immobilized on the fiber-optic surface was demonstrated by Abel et al[9]. Here, the fluorescence intensity was monitored in real time and the biosensor could be regenerated over many cycles by chemical and thermal denaturation. Fiber-optic bundles, each immobilized with a different ssDNA probe on its distal end were used to detect multiple fluorescently labeled ssDNA strands rapidly (< 10 minutes) upto a concentration of 10nM in solution[11]. Other novel systems have been explored with optical transduction such as

bead based arrays where selective chemical etching of the cladding produces microspheres assembled in micro-wells onto which ssDNA probes are attached[12,13].

1.2 ELECTROCHEMICAL TRANSDUCTION

In electrochemical transduction, detection of hybridization is accomplished by electro-active hybridization indicators which interact differently with ssDNA and dsDNA. A variety of molecules can be used as hybridization indicators which bind to dsDNA reversibly through electrostatic binding or intercalation (fitting themselves between the base pairs of dsDNA molecules). Transition metal complexes such as Pt, Ru, Co, and Fe complexes and heterocyclic dyes such as Ethidium Bromide, anthracyclines, phenothiazines, and acridine derivatives, bind reversibly through intercalation. Transition metal complexes of Cobalt ($Co(bpy)_3^{3+}$ and $Co(phen)_3^{3+}$[14], organic dyes such as methylene blue, enzyme labeled DNA probes[15-17] have been successfully implemented to detect DNA hybridization reactions electrochemically. Other electrochemical techniques include labeling with metal nanoparticles, and use of carbon nanotubes for detection of hybridization[18].

Label free electrochemical techniques although not as sensitive as labeled techniques eliminate the need for the label which could simplify the assay. Typically, the oxidation of guanine is monitored during hybridization by cyclic voltammetry[19,20], square wave voltammetry[21], adsorption stripping potentiometry[22], differential pulse voltammetry[23], etc. Label free techniques cause irreversible damage to the immobilized DNA and so are generally not preferred over labeled techniques.

1.3 PIEZOELECTRIC TRANSDUCTION

Piezoelectric biosensors utilize surface acoustic wave based sensors such as the quartz crystal microbalance (QCM) where the quartz crystal resonates at a high frequency. Piezoelectric materials develop an electric potential when mechanical stresses are applied onto it and conversely, when an oscillating electric potential is applied, it vibrates at its resonant frequency. The resonant frequency of the quartz crystal reduces linearly according to the Sauerbrey equation (valid for rigid, thin films only)[24] when any mass is adsorbed onto the surface of the quartz crystal and accurate measurements of the frequency can give mass sensitivities which are in the ng/cm^2 range. QCMs are highly sensitive mass sensors which can be used for mass detection in real time by monitoring the frequency decrease associated with the binding events as they happen. Typically, a ssDNA probe is immobilized onto the surface of the resonator by using thiol chemistry; thiolated ssDNA strands are allowed to bind to form a self assembled monolayer or by using biotin-avidin-biotinylated ssDNA sandwich structures to form a layer of ssDNA molecules on the resonator surface. The complementary strand is allowed to bind to this immobilized probe in solution and the frequency decrease associated with the hybridization is monitored over time. Examples of detection of DNA hybridization using piezoelectric sensors have been demonstrated for the detection of microalgae *Alexandrium minutum* which causes shell fish poisoning[25], *Salmonella typhimurium* [26], *E. coli* genomic DNA[27]. The detection of point mutations by Su et al[28] has been shown where the binding of protein MuTS (which binds to mismatched DNA pairs) can be discriminated for perfectly matched and imperfectly matched DNA hybrids. With energy dissipation monitoring for adsorbed films now available in most

commercially available QCMs, the mass of soft films, where the Sauerbrey equation fails, can be determined accurately[29] making the piezoelectric sensing a robust technique to detect DNA hybridization.

1.4 COLORIMETRIC ASSAYS

Colorimetric techniques utilize reporter particles such as gold nanoparticles (GNPs) to detect the presence of the analyte visually without the need for expensive detectors. This makes this technique very promising to be used in point-of-care diagnostics, especially in developing countries. Colorimetric sensors already have been widely used in pregnancy test strips and in the detection of infectious diseases. DNA based colorimetric techniques rely on color change after the complementary strand hybridizes with GNP labeled ssDNA probes. The resulting polymeric network due to the hybridization reaction changes the color of the dispersed GNPs in solution from red to blue[30,31].

The goal of DNA-based biosensors is the detection of genetic diseases and detection of infectious diseases. The first part of my work deals with the detection of disease causing DNA mutations by making use of the viscoelastic properties of DNA strands and the second portion of my work is on rapid DNA-based diagnostics where isothermal DNA amplification techniques in conjunction with lateral flow assays are used to detect infectious microorganisms in a low cost manner.

2.0 MUTATION SCREENING BASED ON THE MECHANICAL PROPERTIES OF DNA MOLECULES

2.1 INTRODUCTION

The complete sequencing of the human genome has created a tremendous interest in large scale DNA characterization and sequencing[32,33] . With the rapid increase in the number of mutations identified, detection of genetic variations in patients would bring about early diagnosis and even prevention of certain diseases like cancer. The current gold standard for identifying gene mutation is based on DNA sequencing technologies such as the capillary array electrophoresis. However, precisely sequencing a large number of samples is currently time-consuming and expensive. Screening of gene mutations prior to precise mutation identification would significantly reduce the number of samples that need to be sequenced and, therefore, development of rapid, sensitive, and inexpensive technologies for DNA mutation screening is of great interest. Some of the current mutation screening technologies include allele specific oligonucleotides, protein truncation test, DNA microarray technology and electrophoretic mobility shift assays [32,34-39]. Although these screening methods have all been explored to a reasonable degree of success[40], they are limited by the length of the DNA that can be effectively screened per operation, which is apparently an important factor that determines the cost of mutation screening. Among them, the electrophoretic mobility shift assays, including single strand conformational polymorphism (SSCP) and heteroduplex analysis (HA), are able to screen longer DNA strands than other methods and have gain clinical popularity. However, the

maximum length of the DNA that can be effectively screened by SSCP and HA is still limited to be less than 300 base pairs (bps) and the optimization of these electrophoretic mobility shift assays is highly empirical[39].

In this work, we demonstrate another effective approach for rapid gene mutation screening by making use of the mechanical properties of single-strand DNA (ssDNA). It is based on the folding of ssDNA strands in aqueous solution and the immobilization of such strands to a quartz crystal resonator. We show that appreciable differences in the shear modulus can be detected between ssDNA films consisting of wild type and mutant type DNA strands of *p53* gene, due to a single base mutation in a total of 545 bases. We choose to use the *p53* gene and its mutant as an example to demonstrate the capability of this technology, because *p53* gene has been used as examples for other mutation screening technologies[32,34] and its importance has been extensively studied as its mutation leads to cancers such as breast cancer, bone cancer and bladder cancer[41].

2.2 EXPERIMENTAL DETAILS

2.2.1 DNA sample preparation

The gene samples used were *p53* wild type gene and *p53* R type mutant, both containing 1182 bps. A fragment of the genes containing 545 bases was amplified by PCR (**Figure 1**) . By modifying one primer with a biotin group at the 5' end, biotin dsDNA strands were obtained. (**Table 1**). The amplification product was purified to remove the reaction buffer and the primers. The purified dsDNA was denatured at 95°C and cooled suddenly at -20°C to form ssDNA, with one strand containing biotin at the 5' end and the other strand containing the complementary base sequence to the biotinylated strand. 100 μL of the purified ssDNA was diluted in 1.5 mL of phosphate buffered saline (PBS, pH 7.4) and this formed the sample that was introduced to the quartz crystal resonator.

Table 1. PCR primers for amplification of *p53* wild type and R type mutant genes:

Primer name	Primer Sequence
Forward primer	5'-biotin-TCATCTTCTGTCCCTTCCC-3'
Backward primer	5'-CAAACACGCACCTCAAAG-3'

a. *p53* wild type gene sequence

```
1    ATGGAGGAGC CGCAGTCAGA TCCTAGCGTC GAGCCCCCTC TGAGTCAGGA AACATTTTCA
61   GACCTATGGA AACTACTTCC TGAAAACAAC GTTCTGTCCC CCTTGCCGTC CCAAGCAATG
121  GATGATTTGA TGCTGTCCCC GGACGATATT GAACAATGGT TCACTGAAGA CCCAGGTCCA
181  GATGAAGCTC CCAGAATGCC AGAGGCTGCT CCCCGCGTGG CCCCTGCACC AGCAGCTCCT
241  ACACCGGCGG CCCCTGCACC AGCCCCCTCC TGGCCCCTGT CATCTTCTGT CCCTTCCCAG
301  AAAACCTACC AGGGCAGCTA CGGTTTCCGT CTGGGCTTCT TGCATTCTGG GACAGCCAAG
361  TCTGTGACTT GCACGTACTC CCCTGCCCTC AACAAGATGT TTTGCCAACT GGCCAAGACC
421  TGCCCTGTGC AGCTGTGGGT TGATTCCACA CCCCCGCCCG GCACCCGCGT CCGCGCCATG
481  GCCATCTACA AGCAGTCACA GCACATGACG GAGGTTGTGA GGCGCTGCCC CCACCATGAG
541  CGCTGCTCAG ATAGCGATGG TCTGGCCCCT CCTCAGCATC TTATCCGAGT GGAAGGAAAT
601  TTGCGTGTGG AGTATTTGGA TGACAGAAAC ACTTTTCGAC ATAGTGTGGT GGTGCCCTAT
661  GAGCCGCCTG AGGTTGGCTC TGACTGTACC ACCATCCACT ACAACTACAT GTGTAACAGT
721  TCCTGCATGG GCGGCATGAA CCGGAGGCCC ATCCTCACCA TCATCACACT GGAAGACTCC
781  AGTGGTAATC TACTGGGACG GAACAGCTTT GAGGTGCGTG TTTGTGCCTG TCCTGGGAGA
841  GACCGGCGCA CAGAGGAAGA GAATCTCCGC AAGAAAGGGG AGCCTCACCA CGAGCTGCCC
901  CCAGGGAGCA CTAAGCGAGC ACTGCCCAAC AACACCAGCT CCTCTCCCCA GCCAAAGAAG
961  AAACCACTGG ATGGAGAATA TTTCACCCTT CAGATCCGTG GGCGTGAGCG CTTCGAGATG
1021 TTCCGAGAGC TGAATGAGGC CTTGGAACTC AAGGATGCCC AGGCTGGGAA GGAGCCAGGG
1081 GGGAGCAGGG CTCACTCCAG CCACCTGAAG TCCAAAAAGG GTCAGTCTAC CTCCCGCCAT
1141 AAAAAACTCA TGTTCAAGAC AGAAGGGCCT GACTCAGACT GA
```

b. *p53* R type mutant gene sequence (R175H G-A)

```
1    ATGGAGGAGC CGCAGTCAGA TCCTAGCGTC GAGCCCCCTC TGAGTCAGGA AACATTTTCA
61   GACCTATGGA AACTACTTCC TGAAAACAAC GTTCTGTCCC CCTTGCCGTC CCAAGCAATG
121  GATGATTTGA TGCTGTCCCC GGACGATATT GAACAATGGT TCACTGAAGA CCCAGGTCCA
181  GATGAAGCTC CCAGAATGCC AGAGGCTGCT CCCCGCGTGG CCCCTGCACC AGCAGCTCCT
241  ACACCGGCGG CCCCTGCACC AGCCCCCTCC TGGCCCCTGT CATCTTCTGT CCCTTCCCAG
301  AAAACCTACC AGGGCAGCTA CGGTTTCCGT CTGGGCTTCT TGCATTCTGG GACAGCCAAG
361  TCTGTGACTT GCACGTACTC CCCTGCCCTC AACAAGATGT TTTGCCAACT GGCCAAGACC
421  TGCCCTGTGC AGCTGTGGGT TGATTCCACA CCCCCGCCCG GCACCCGCGT CCGCGCCATG
481  GCCATCTACA AGCAGTCACA GCACATGACG GAGGTTGTGA GGCACTGCCC CCACCATGAG
541  CGCTGCTCAG ATAGCGATGG TCTGGCCCCT CCTCAGCATC TTATCCGAGT GGAAGGAAAT
601  TTGCGTGTGG AGTATTTGGA TGACAGAAAC ACTTTTCGAC ATAGTGTGGT GGTGCCCTAT
661  GAGCCGCCTG AGGTTGGCTC TGACTGTACC ACCATCCACT ACAACTACAT GTGTAACAGT
721  TCCTGCATGG GCGGCATGAA CCGGAGGCCC ATCCTCACCA TCATCACACT GGAAGACTCC
781  AGTGGTAATC TACTGGGACG GAACAGCTTT GAGGTGCGTG TTTGTGCCTG TCCTGGGAGA
841  GACCGGCGCA CAGAGGAAGA GAATCTCCGC AAGAAAGGGG AGCCTCACCA CGAGCTGCCC
901  CCAGGGAGCA CTAAGCGAGC ACTGCCCAAC AACACCAGCT CCTCTCCCCA GCCAAAGAAG
961  AAACCACTGG ATGGAGAATA TTTCACCCTT CAGATCCGTG GGCGTGAGCG CTTCGAGATG
1021 TTCCGAGAGC TGAATGAGGC CTTGGAACTC AAGGATGCCC AGGCTGGGAA GGAGCCAGGG
1081 GGGAGCAGGG CTCACTCCAG CCACCTGAAG TCCAAAAAGG GTCAGTCTAC CTCCCGCCAT
1141 AAAAAACTCA TGTTCAAGAC AGAAGGGCCT GACTCAGACT GA
```

Figure 1. Sequences of **a)** *p53* wild type and **b)** R type mutant genes. All the bases between the two primers (marked in red) are amplified by PCR. The total number of amplified bases is 545 for both the *p53* wild and R type mutant. On line 481, three bases are highlighted in black to indicate the position of the mutation: the three highlighted bases are CGC in the wild type and CAC in the R type mutant.

2.2.2 Crystal preparation

The gold-coated quartz crystals having a fundamental resonant frequency of 5 MHz were first cleaned in an ultra violet ozone chamber for 10 minutes and then cleaned in a 5:1:1 mixture of deionized water, ammonium hydroxide, and sodium peroxide at 74°C for 5-8 minutes. They were then washed with deionized water and dried with nitrogen gas. It was again placed in the UV ozone chamber for 10 minutes to oxidize any organic impurities present on the crystal surface before the surface was modified with the biotin-thiol molecule.

2.2.3 Formation of the biotin-thiol, streptavidin and ssDNA layers and data collection

The crystals were soaked overnight in a solution of biotin-terminated tri(ethylene glycol)hexadecanethiol (concentration of 1 mM in anhydrous ethanol). They were then washed three times with anhydrous ethanol and deionized water and dried with nitrogen gas. A monolayer of the biotin-thiol was deposited onto the surface via a covalent bond between the thiol group and the gold. The biotin end of the molecule was directed away from the surface forming a biotin surface on the crystal (**Figure 2a**). The resonant frequency and energy dissipation data were collected and processed by a commercial module (Q-sense E1). All measurements were made in PBS (pH 7.4) at a constant temperature of 23°C. The crystals were checked for the resonant frequency for odd harmonic resonances (1 to 13) in the aqueous phase before any measurements were made. The flow rate of PBS was kept at 200 µl/min. After obtaining a stable frequency baseline in PBS, streptavidin (1 µM in PBS, purchased from Sigma Aldrich) was flowed over the crystal (**Figure 2b**). The fast irreversible binding of streptavidin and biotin was confirmed by a sharp decrease in the resonate frequency of the crystals. The

biotinylated ssDNA sample was then flowed over the streptavidin layer to which the biotin end of the ssDNA binds (**Figure 2c and 2d**).

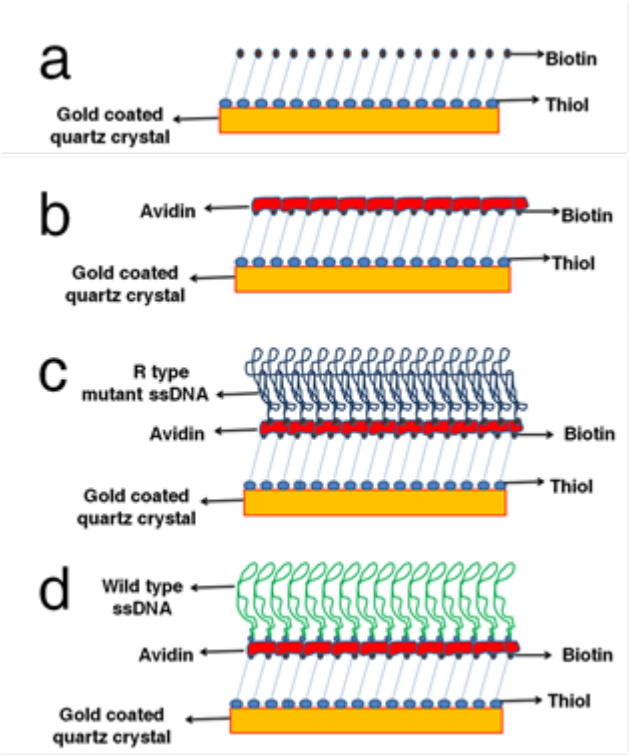

Figure 2. Schematic process for immobilizing ssDNA strands with a complex 3-D structure on a quartz crystal **a)** A monolayer of biotin-thiol is immobilized onto the Au film by covalently linking the thiol group to Au. **b)** A layer of streptavidin binds to the biotin layer. **c)** Biotinylated mutant type ssDNA with a complex 3-D structure is immobilized through binding with the streptavidin layer. **d)** Biotinylated wild type ssDNA (with a different 3-D structure from the mutant type) is immobilized onto the crystal by the same method.

2.3 RESULTS AND DISCUSSION

The scheme for immobilizing ssDNA stands, amplified from either the wild type or mutant type, on the surface of the resonator is presented in **Figure 2**. The quartz crystal resonator is coated with a thin gold (Au) film. A monolayer of biotin modified with a thiol functional group (biotin-thiol) is first immobilized onto the Au film by covalently linking the thiol group to Au (**Figure 2a**). A layer of streptavidin then binds to the biotin layer (**Figure 2b**). Afterwards, ssDNA with a biotin group at the 5' end (biotinylated ssDNA) is immobilized through binding with the streptavidin layer (**Figure 2c** and **Figure 2d**). The biotinylated ssDNA is produced by amplifying a fragment of the *p53* gene with a biotin-modified primer, followed by denaturing the amplified dsDNA at 95^{o}C and suddenly cooling at -20°C. Upon the sudden temperature quench, each ssDNA strand undergoes intra-base pairing and forms a particular complex 3-D structure which is characteristic of its base sequence. Because of the presence of the mutant base, ssDNA strands amplified from wild type and mutant type genes form different 3D conformations before they are tethered to the surface of the resonator, which would eventually result in films of different mechanical properties.

The quartz crystal resonator is driven at its fundamental resonant frequency of 5 MHz in PBS buffer. The odd harmonic resonances with resolution down to 1 Hz and the energy dissipation of the resonator are recorded as a function of time. The energy dissipation is given in

terms of the dissipation factor D[42] which is inversely proportional to the quality factor (Q) and defined in terms of energy dissipated versus energy stored in the oscillator as:

$$D = \frac{1}{Q} = \frac{\text{Energy dissipated per oscillation}}{2\pi \text{ Energy stored in the oscillator}} \quad \textbf{(1)}$$

Figure 3 shows a typical response of the fifth harmonic frequency (**Figure 3a** and **Figure 3b**) and the energy dissipation (**Figure 3c and Figure 3d**) of the resonator recorded during the immobilization of wild type and mutant type ssDNA strands respectively. The first sharp decrease in the resonant frequency and the slight increase in energy dissipation indicate a strong binding of streptavidin to the biotin layer on the crystal. The biotin on the crystal binds to two of the four binding sites of each streptavidin molecule, thus forming a reasonably rigid layer[43,44]. Upon flowing the ssDNA sample over the crystal, the biotin end of the ssDNA quickly binds to the streptavidin present on the crystal surface. This is seen as a large decrease in frequency and a more apparent increase in energy dissipation. For both the wild and mutant type ssDNA, the frequency decrease due to binding of the ssDNA (**Figure 3a and Figure 3b**) is about the same, indicating that the mass adsorbed is about the same. This is expected as the number of bases for the wild type and the mutant type ssDNA are both 545 bases. However, interestingly, appreciable differences in the energy dissipation due to binding of the wild type (**Figure 3c**) and the mutant type (**Figure 3d**) are observed, indicating that the viscoelastic properties of the films consisting of the two types of ssDNA strands are different.

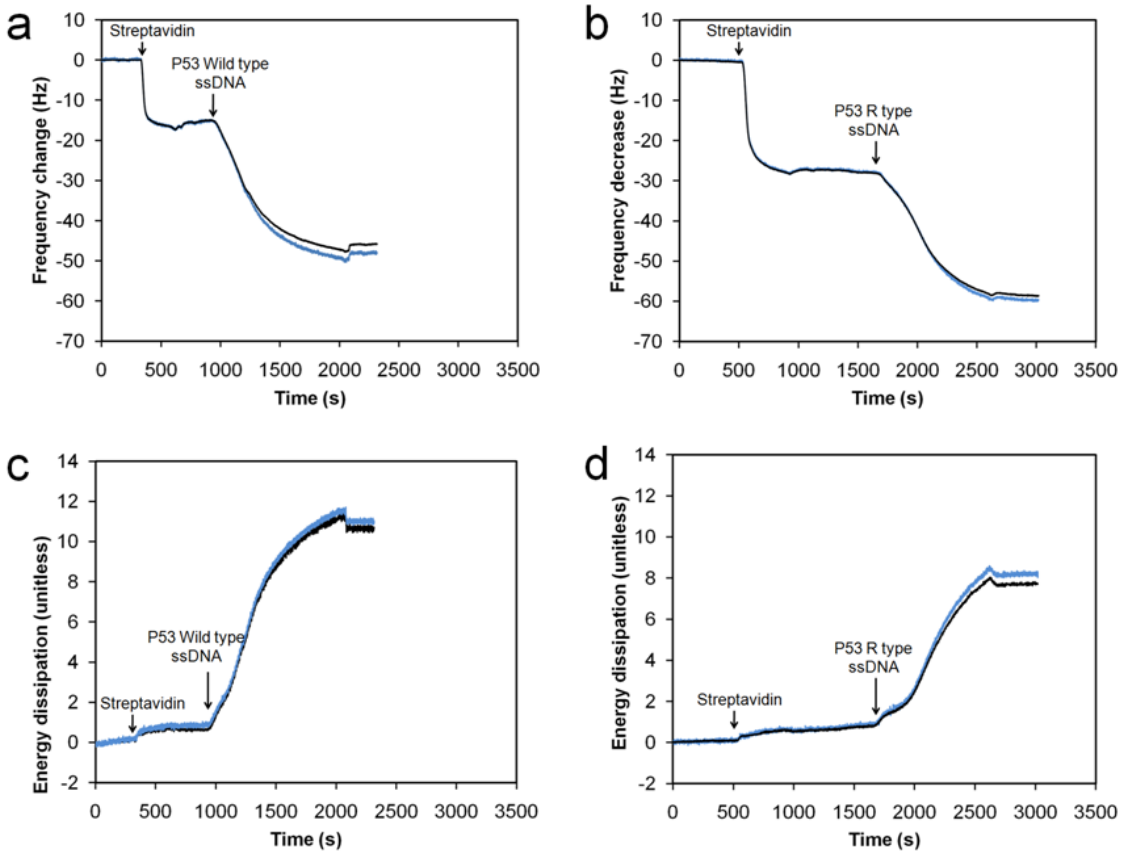

Figure 3. Plot of raw (*blue curve*) and fitted (*black curve*) data for a typical frequency response and energy dissipation of the resonator at its fifth harmonic resonance as a function of time during the immobilization of the streptavidin layer and the ssDNA film. **a)** Frequency response plot for the wild type sample. **b)** Frequency response plot for the mutant type sample. **c)** Energy dissipation plot for the wild type sample. **d)** Energy dissipation plot for the mutant type sample.

To extract the viscoelastic properties of the ssDNA films from the frequency response and energy dissipation of the resonator, the film is modeled using the Voight model of viscoelasticity. The Voight model is represented as a spring and a dashpot in parallel, the spring constituting the pure elastic response and the dashpot, the viscous response. The calculation of shear modulus of polymer films from the electrical response of the quartz resonator using transmission line analysis has been well investigated earlier[45-47]. A more direct method is the

continuum mechanics approach, in which the materials physical properties such as the film shear modulus, film viscosity, and film thickness are directly related to the experimentally measured resonant frequency change and the energy dissipation response[48]. Within the framework of continuum mechanics, the shear modulus used in the Voight model is a complex shear modulus (μ^*) which can be written as:

$$\mu^* = \mu + i2\pi f\eta, \tag{2}$$

where μ is the elastic shear modulus and η is the shear viscosity of the film. For viscoelastic materials, as the strain lags the stress by some amount, describing this behavior by a complex shear modulus makes it convenient to separate out the in-phase and out-of-phase stress components[46]. When a shear stress σ_{xy} is applied to the film, the stress strain relationship on the Voight element is given as follows[48]:

$$\sigma_{xy} = \mu\frac{\partial u_x(y,t)}{\partial y} + \eta\frac{\partial v_x(y,t)}{\partial y} \tag{3}$$

where u_x is the displacement in the x direction and v_x is the velocity in the x direction. μ, η, and the thickness of the film can be obtained by solving the wave equation for the propagation of bulk shear waves in a viscoelastic medium using appropriate boundary conditions[48,49] at each layer on the crystal surface and fitting the frequency response and energy dissipation into the model. The fitted frequency response and energy dissipation of the resonator according to this model are plotted and compared with the raw data in **Figure 3,** which shows reasonably good agreement.

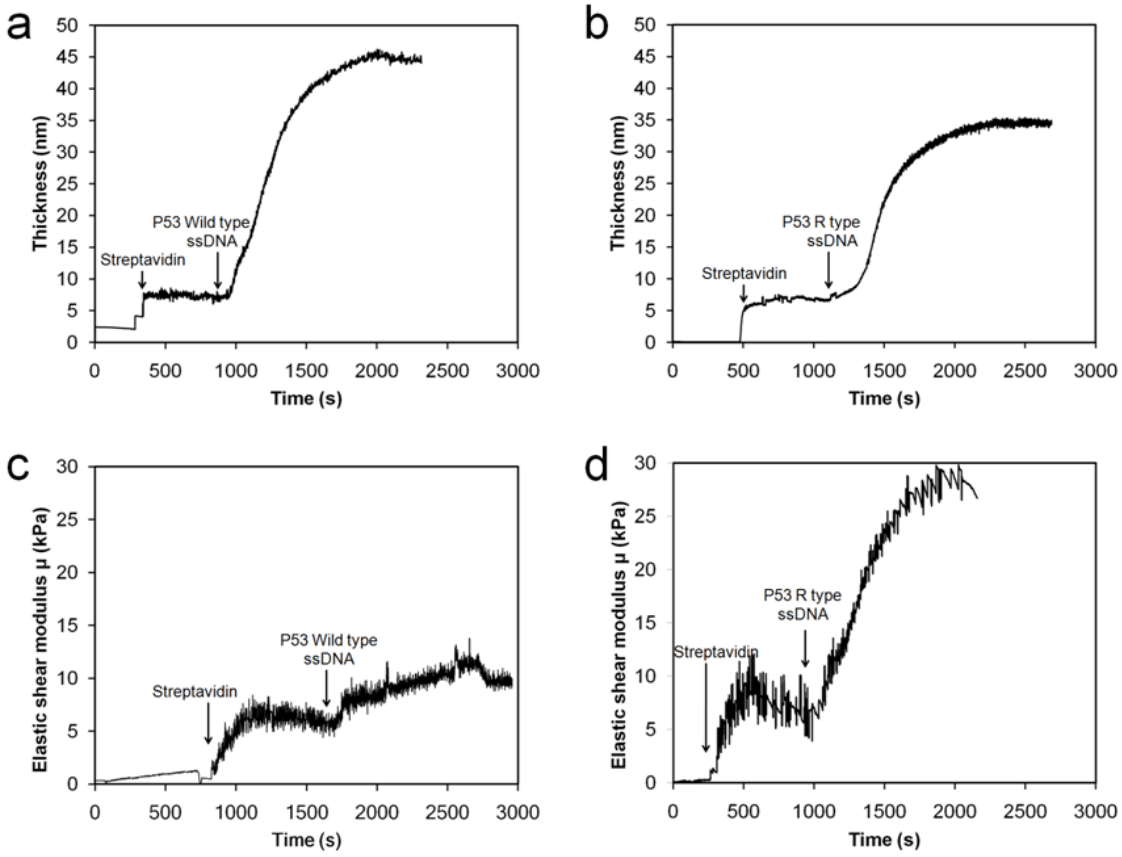

Figure 4. Plot of thickness and elastic shear modulus (μ) of ssDNA films obtained from the data in **Figure 3**. **a)** Film thickness as a function of time for the wild type ssDNA sample. **b)** μ as a function of time for the wild type sample. **c)** Film thickness as a function of time for the mutant type sample. **d)** μ as a function of time for the mutant type sample.

Figure 4 plots the thickness and μ of the films obtained from fitting the Voight model to the raw data. It is obvious that an appreciable difference in the plots of μ can be observed between the two types of samples, although the difference in the plot of film thickness is insignificant. The most apparent difference in the plot of μ is that after the DNA strands are immobilized, μ is about 11 kPa for the wild type sample but is about 28 kPa for the mutant type one. To confirm the result, the experiments for both types of samples are each repeated four times, and the result is presented in **Table 2**. It is found that the thickness of the biotin-streptavidin layer is about 10.0 nm with a standard deviation of 1.6 nm, the total thickness of the

film after immobilizing the wild type ssDNA is about 30.0 nm with a standard deviation of 5.6 nm, and the total film thickness for the mutant type ssDNA is about 36 nm with a standard deviation of 3.7 nm. This indicates that no significant difference in the film thickness can be observed between the two types of samples, and the two types of DNA strands are immobilized on the surface with a similar aerial mass density consistently from experiment to experiment. However, μ of the films with immobilized wild type samples is about 13,715 Pa with a standard deviation of 1,713 Pa, while μ of the films with immobilized mutant type samples is about 24,399 Pa with standard deviation of 1,808 Pa.

The large difference in μ indicates that there is an appreciable difference in the viscoelasticity of the films formed by the wild type and mutant type DNA. This difference is likely because the two types of ssDNA strands form different 3-D conformations in aqueous solution which is the direct result of one base mutation in their sequences. Upon quenching the temperature rapidly, ssDNA strands form a complex 3-D structure to minimize its free energy and hybridize with itself via intra-base pairing. During this process, even a single base mutation may significantly alter the 3-D structure of the ssDNA in solution, which leads to the appreciable differences in the mechanical properties of the DNA films formed by tethering such DNA strands to a solid surface. The resulted difference in the mechanical properties of the DNA films may be detected by a number of techniques. We believe that the example we show here by probing the elastic shear modulus of the DNA films using a quartz crystal resonator is only one approach among many others.

Table 2. Film thickness and shear modulus measured during the immobilization of *p53* wild type ssDNA and the *p53* R type mutant ssDNA.

Sample		**Film thickness: (nm)**	**Film Shear Modulus (Pa)**
***p53* Wild type ssDNA**	Expt 1	29.5	15,561
	Expt 2	37.6	14,553
	Expt 3	21.9	10,953
	Expt 4	31.0	13,793
***p53* R type mutant ssDNA**	Expt 1	35.9	25,542
	Expt 2	34.3	23,258
	Expt 3	42.1	26,687
	Expt 4	32.1	22,110

2.4 CONCLUSIONS

Although resonator-based sensors have been used for mutation detection [28,29,50-53], they are all based on mass change on the surface of the resonator which serves as a mass balance. Such mass change is typically caused by capturing DNA strands through hybridization with a DNA probe or use of a bioreceptor. To the best of our knowledge, no literature has reported mutation screening based on the mechanical properties of the ssDNA films. Coupling DNA films with a resonator provides an excellent means to probe the mechanical properties of DNA films. Combining it with the capability of DNA molecules to form unique 3-D structures enables us to screen the mutant from wild type DNA quickly and reliably. We have shown the capability of this technique to detect a single base mutation among a fragment of 545 bases in *p53* gene, which already exceeds the reported maximum length of the DNA that can be effectively screened by other methods such as SSCP/HA and its variants. This technique can be further improved by selecting different fragments of the gene containing the mutation to optimize the screening. Similar to all the technologies based on the formation of DNA 3-D complex structures, much study still needs to be carried out to understand and predict the 3-D structure of the long DNA strand in solution as well as on a solid surface, so that better experiments could be designed to maximize the difference in the mechanical properties of the 3-D structures between the wild and mutant type DNA.

3.0 RAPID DNA-BASED DETECTION OF INFECTIOUS DISEASES

3.1 NEED FOR RAPID DIAGNOSTIC ASSAYS

The tremendous advancements made in the healthcare industry especially in the area of rapid and reliable diagnosis of diseases have not fully reached the developing and the under-developed countries. The need for rapid point of care diagnostics is booming in the developing world largely due to the interest shown by the developed countries and world organizations such as the WHO to make basic healthcare accessible to the poorest regions of the world. For example, the number of child deaths (below 5 years of age) in the year 2008 was estimated to be about 8.8 million with more than 90% of the deaths occurring in South Asia and Africa. Pneumonia and diarrhea account for a third of these deaths. Moreover, children severely affected by malnutrition are at a high risk of death due to diarrhea and pneumonia making these the deadliest diseases leading to child mortality in the developing world. Although improvements in public health care such as better sanitation and safe drinking water are of paramount importance to prevent their occurrence, rapid diagnosis of these diseases which are otherwise very treatable is very essential. Life threatening diseases such as Gonorrhea and Chlamydia which are highly prevalent in the poorest regions of the world could be easily cured if diagnosed correctly at the right time.

Ideally point of care diagnostic procedures aimed for the developing world should have the following characteristics:

a) **Sensitive and specific:** The test should be able to detect all the positives and give few false positives.

b) **Affordable:** The test should not require large, expensive machinery and should be administered to the public at a low cost.

c) **Rapid:** The results of the test should be made available rapidly, typically in only one sitting so that treatment can be carried out immediately.

d) **Simple to use:** The test should be designed in a way such that inexperienced personnel should be able to operate it without too much difficulty.

Conventionally, DNA-based biosensors are based on hybridization of the complementary strand to an immobilized ssDNA probe. Biosensors based on DNA hybridization suffer from slow hybridization kinetics when compared to hapten-antibody or antibody-antigen binding kinetics. Also, many incomplete hybridization reactions between not fully complementary strands produce false positive signals because although not fully complementary, the sequences may contain significant portions of complementary sequences. Furthermore, the amount of DNA material available from patient samples is typically low and amplification is usually necessary. DNA amplification with optimally designed primers labeled with haptens such as biotin, FITC, Digoxigenin, etc. amplify the DNA with high specificity and the presence of the label makes it easy to detect via hapten-antibody reactions using low cost methods such as detection via lateral flow strips.

Therefore, the success of the DNA biosensor primarily depends on the design of primers, which provides the selectivity and the sensitive detection of the labels which is largely dependent on the right antibody immobilization technique. We thought it would be worthwhile to investigate the right antibody immobilization method for biosensor applications before we delve into the detection of amplified DNA products.

3.2 CHARACTERIZATION OF ANTIBODY IMMOBILIZATION METHODS

3.2.1 Introduction

Biosensors sensors which incorporate antibodies to detect the target molecule (analyte) find applications in numerous fields such as medical diagnostics, environmental applications and food analysis to name a few [54-56]. The high specificity, sensitivity and rapid detection times have rightly warranted great interest in the field of antibody based biosensors. The specificity of antibodies to single out the target molecule from a complex medium is the biggest driving force to engineer antibody based biosensors. But, the reliability of antibody based biosensors has been a major issue as immobilization of the antibodies on substrates tends to make them inactive, as a result of which the antibody loses its 'biosensing' ability. The reasons for inactivity could be due to the denaturing of the antibodies on the surface or because of the unfavorable orientation of the surface antibodies wherein the antibody is unable to bind to the antigen. With different populations of the immobilized antibodies rendered inactive, the sensitivity becomes inconsistent and it also becomes difficult to study the kinetics of the antibody-antigen interaction [57]. These factors are major hindrances to the development of sensitive, miniaturized biosensors.

Antibodies contain two light chains and two heavy chains which form a "Y" shaped structure [58]. The amino acid sequence at the tips of the "Y" shaped antibody molecule, for both the heavy chain as well as the light chain, is variable, which gives it the high affinity and specificity to bind to the antigen. The Fc region of the antibody contains carbohydrate molecules which could be used to anchor the antibody to substrates in a way that the antigen binding domain is free to bind antigen. Immobilization of the antibodies by physical adsorption using the

van der Waal's forces is probably the simplest, but studies have shown that antibodies denature when immobilized this way [59,60]. Immobilizing antibodies by covalent attachment [61-63] to surfaces is robust and efficient, but may cause denaturing or the antibody may be immobilized with its active sites blocked.

A number of research articles have been written confirming that oriented immobilization of antibodies is better suited to capture antigens than randomly oriented antibodies[64-68]. The kinetic rate constants of antibody-antigen interactions have been studied using labeled techniques such as fluorescence based fiber-optic biosensor[57], TMB substrate assay[69] and label free techniques such as surface plasmon resonance (SPR)[70] and quartz crystal microbalance (QCM)[63,71], but to our knowledge, none have described the equilibrium binding kinetics in detail. The choice of the right immobilization method for biosensor applications depends not only on the amount of freely available antibodies on the surface [Ab_o] and the association equilibrium constant K_a, but also on the concentration of the antigen that needs to be detected. The QCM's real time mass sensitivity, reliability and ease of surface modification make it an excellent choice to probe the equilibrium kinetics of antibody-antigen binding. It can measure extremely low masses (ng/cm^2) with very high precision by accurately measuring the decrease in the resonant frequency of the quartz crystal when mass is deposited on it. The frequency of resonance of the quartz crystal decreases linearly with the mass adsorbed according to the Sauerbrey equation and a very accurate and sensitive measurement of mass adsorbed can be made.

In this work, we examine some of the most commonly used techniques to immobilize antibodies and provide a quantitative means to evaluate the different immobilization chemistries and their associated heterogeneities when immobilized. We have studied the immobilization of Mouse IgG antibody (antibody) via three different immobilization schemes and its interaction with Anti-Mouse IgG antibody (antigen). Mouse IgG antibodies were immobilized by covalent attachment to the substrate (randomly oriented), attachment via Protein A which specifically

binds to the Fc region of the antibody (partially oriented) and finally, attachment by biotinlyated antibody to a streptavidin covered substrate (fully oriented). Equilibrium adsorption studies were conducted for each of the immobilization chemistries using the QCM. The equilibrium adsorption isotherm between the antibody and antigen follows the conventional Langmuir adsorption model, from which we can obtain useful information about the association equilibrium constant (K_a) and the surface concentration ($[Ab_o]$) of active antibody. Also, the equilibrium data has been fitted to the Sips isotherm from which we can gain information about the surface heterogeneity of the immobilized antibody and the validity of the Langmuir isotherm. The Sips isotherm also provides us with the K_a and $[Ab_o]$ for the adsorption experiments. From the results of our work, it is evident that the best method of immobilization depends not only on the amount of freely available active binding sites on the surface and the association equilibrium constant which are totally dependent on the immobilization method, but also on the concentration range of the antigen. For lower concentrations of the antigen, we find that the three methods of immobilization are comparable, whereas for higher antigen concentrations, oriented immobilization gives better results.

3.2.2 Experimental details

Materials

Mouse IgG antibody, Antimouse IgG antibody produced in goat, Protein A from Staphylococcus aureus, streptavidin were purchased from Sigma Aldrich Chemicals, MO. Biotin-PEG4-Hydrazide and Dithiobis succinimidylpropinonate (DSP) was purchased from Thermo Fischer. Biotin-terminated tri (ethylene glycol)hexadecanethiol was purchased from Assemblon. Gold coated quartz crystals having a resonance frequency of around 5 MHz were purchased from Q-sense. Dimethylsulfoxide (DMSO) was purchased from Fisher chemicals, Phosphate buffer saline (PBS) was used throughout unless specified. Ammonium hydroxide and sodium peroxide solutions were used to clean the gold coated quartz crystals.

Crystal preparation and data collection

The gold coated quartz crystals were cleaned by first placing them in a UV ozone chamber for 15 minutes to oxidize any organic impurities present on the surface. It was then treated with a 5:1:1 solution of deionized water, ammonium hydroxide and sodium peroxide at 74 ^{o}C for 10 minutes. The crystals were washed with DI water and placed in the UV ozone chamber for another 10 minutes before any surface modification was made. The resonant frequency of the quartz crystal was measured in a commercial QCM (Q-sense E1). All experiments were carried out in PBS at a flowrate of 100 µL/min at 23^{0} C. The crystals were checked for the resonant frequency for the odd harmonics (1 to 13) in PBS and the frequency was allowed to stabilize before the adsorption data was collected.

Direct covalent immobilization

Covalent attachment of proteins to surfaces like glass or gold is rapid and inexpensive. It can be carried out by amine chemistry (by functionalizing the surface with active NHS esters or aldehydes), thiol chemistry (by maleimide, disulfide or vinyl sulfone functionalized surfaces) or by carboxyl chemistry using carbodiimde activation [61,62,72]. Mouse IgG antibody was covalently immobilized on the gold coated quartz crystal using amine chemistry by functionalizing the gold surface of the quartz crystal with active NHS ester groups. The disulfide linkage in DSP rapidly attaches to the gold surface and the NHS ester moiety reacts with the free amine groups present on the antibody surface to form stable amide bonds. The cleaned gold coated quartz crystals are immersed in DSP at a concentration of 4 mg/mL in DMSO for 30 minutes at room temperature and then rinsed with DMSO and water three times. It is then immediately immersed in the antibody solution (Mouse IgG) of concentration 0.05 mg/mL for 4 hours to link it to the gold surface. The gold crystals are then washed with PBS buffer to remove the cross linker byproducts and the unconjugated antibody before being loaded into the QCM. The scheme of immobilization of the antibody via covalent attachment is presented in **Figure 5a**. Antigen solutions (Antimouse IgG produced in goat) of concentrations ranging from 1 nM to 100 nM are allowed to bind to the Mouse IgG present on the surface. After the binding has reached equilibrium, it is washed with PBS and the amount of antigen bound on the surface for each concentration of the antigen in solution is evaluated by measuring the decrease in the resonant frequency of the QCM.

Immobilization via Protein A

Protein A is a coat protein extracted from the bacterium Staphylococcus aureus which can specifically bind to the Fc region of IgG class of antibodies. Although Protein A, Protein G and Protein L all exhibit specific binding to IgG class of antibodies, Protein A was chosen to immobilize Mouse IgG antibody as it binds to Mouse IgG strongly whereas its binding to the Antimouse IgG antibody produced in goat is weak. This reduces the possibility of Antimouse IgG antibody to bind to the some unbound Protein A sites on the surface. As Protein A binds to the Fc region of the antibody specifically, the antigen binding domain of the antibody is free to bind to the antigen. This makes this scheme of immobilization more oriented with respect to the antibody as opposed to immobilizing the antibody randomly on the crystal surface (**Figure 5b**). Protein A is covalently attached to the gold coated quartz crystal using amine chemistry as described in detail previously. The crystal with Protein A immobilized on the surface is loaded into the QCM's flow module and antibody (Mouse IgG) solution of concentration 0.05 mg/mL is allowed to bind to the Protein A. Once the surface is saturated, antigen (Antimouse IgG antibody) solutions of concentrations ranging from 1 nM to 100 nM are allowed to bind to the antibody present on the surface and the data is evaluated as before.

Immobilization via biotinylated antibody on a streptavidin coated surface

Biotin is a B-complex vitamin molecule which has a very strong affinity for the protein streptavidin and its variants avidin and neutravidin. Biotin can be specifically attached to the Fc region of the antibody [57,73] and when the antibody is immobilized onto a streptavidin coated surface, the antigen binding domain of the antibody is free to bind to the antigen. Carbohydrates are present on the antibody's Fc region which can be oxidized to form aldehydes which when reacted with biotin hydrazide, labels the antibody with biotin specifically at the Fc region. The

detailed protocol to label the antibody with biotin can be found with Thermo Fisher. Instead of using 2 mg/mL of the protein solution, 0.05 mg/mL of antibody (Mouse IgG) solution in PBS was used. Cleaned gold coated quartz crystals were soaked overnight in a solution of biotin-terminated tri (ethylene glycol)hexadecanethiol at a concentration of 1 mM in anhydrous ethanol. A self assembled monolayer (SAM) of the biotin-thiol is deposited via a covalent bond between the thiol and the gold surface with the biotin moiety directed away from the surface forming a monolayer of biotin on the crystal surface (**Figure 5c**). The crystal with the SAM was loaded into the flow module of the QCM and streptavidin of concentration 1 μM in PBS was allowed to bind to the biotin on the crystal surface. The biotin on the crystal binds to two of the four binding sites of each streptavidin molecule, thus forming a reasonably rigid layer [44,74]. The excess streptavidin was washed by rinsing with PBS and the biotinylated antibody (Mouse IgG), concentration 0.05 mg/mL was flowed over the streptavidin layer to which it binds rapidly and irreversibly. It is rinsed again to remove any loosely bound antibody and then antigen (Antimouse IgG antibody) of concentrations ranging from 1 nM to 120 nM are allowed to bind to the Mouse IgG present on the surface and the data was evaluated.

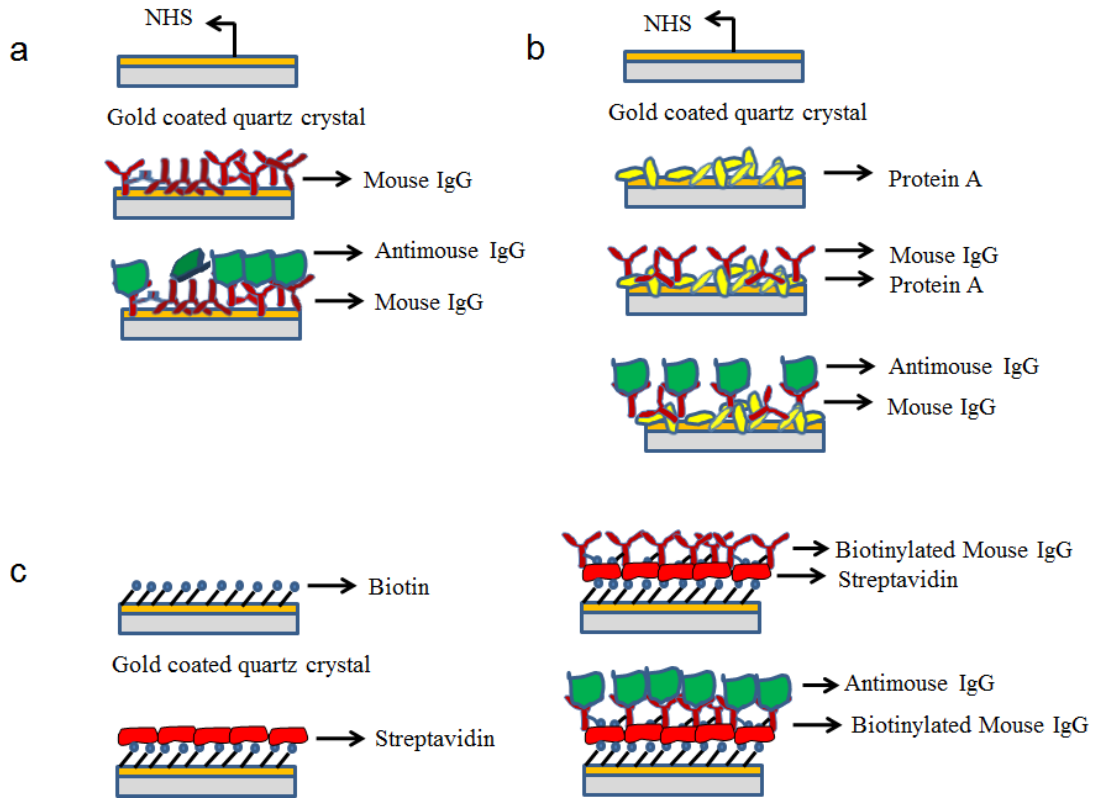

Figure 5. Schematic of the immobilization chemistries **a)** Direct covalent immobilization of the antibodies (Mouse IgG) on the crystal surface. The crystal surface is first functionalized with NHS ester and the antibodies are immobilized randomly on the surface. Antigen (Antimouse IgG) binds to only those antibodies which have favorable orientation. **b)** Immobilization of the antibodies (Mouse IgG) on the crystal surface via Protein A. The crystal surface is first functionalized with NHS ester and Protein A is immobilized randomly on the surface. Antibodies (Mouse IgG) bind specifically at the Fc region to the Protein A. Antigen (Antimouse IgG) binding is more efficient as the antibodies have their antigen binding domain free. **c)** A self assembled monolayer of biotin thiol is formed on the crystal surface onto which streptavidin binds. The antibodies (Mouse IgG) are labeled with biotin at the Fc region which then binds to the streptavidin on the surface. Antigen binding (Antimouse IgG) is depicted in the last schematic.

3.2.3 Results and discussion

Sauerbrey equation to estimate the adsorbed mass

The Sauerbrey equation relates the amount of mass adsorbed onto the quartz crystal linearly with the resonant frequency decrease of the quartz crystal. It is given as:

$$\Delta f = \frac{-2 f_0^2}{A\sqrt{\rho_q \mu_q}} \Delta m \qquad \textbf{(4)}$$

where f_o is the resonant frequency in Hz, Δf is the frequency change in Hz, Δm is the mass change in grams, A is the piezoelectrically active crystal area in cm^2, ρ_q is the density of quartz (ρ_q = 2.648 g/cm^3) and μ_q is the shear modulus of quartz for AT-cut crystal (μ_q =2.947x10^{11} $g/cm.s^2$).

The above equation is only valid when the adsorbing film is thin when compared to the thickness of the quartz [75]. Protein films are generally soft films which dissipate energy through them as the film is not completely coupled to the quartz crystal. But when the dissipation factor (D factor), which is a measure of the energy dissipated through the film is not high it is sufficient to use the Sauerbrey equation to estimate the mass adsorbed. The Sauerbrey equation is applied to the 5^{th} overtone of the resonant frequency of the quartz crystal and the mass adsorbed is calculated in ng/cm^2.

Adsorption isotherms

The equilibrium adsorption for antibody-antigen (Ab-Ag) binding can be very conveniently described by the Langmuir adsorption isotherm. The Langmuir adsorption isotherm is very useful to describe monolayer adsorption which is limited by the equilibrium between the concentration of the species in solution and the concentration of the species adsorbed on the surface. In addition to a monolayer adsorption, the Langmuir isotherm assumes that each binding site can accommodate only one molecule and all the sites are energetically equivalent with no interaction between the species adsorbed. The Langmuir isotherm relates the concentrations of the species adsorbed to the concentration of the species in solution in the following way:

Ab: Antibody, Ag: Antigen, $AbAg^*$ is the Antibody-Antigen complex

$$Ab + Ag \rightarrow AbAg^* \quad \textbf{(5)}$$

$$r_f = k_{on}[Ab][Ag] \quad \textbf{(6)}$$

$$r_b = k_{off}[AbAg]^* \quad \textbf{(7)}$$

where k_{on} is the association kinetic constant and k_{off} is the dissociation kinetic constant.

At equilibrium, $r_f = r_b$ and defining the association equilibrium constant $K_a = k_{on} / k_{off}$,

we have:

$$K_a = \frac{[AbAg]^*}{[Ab][Ag]} \quad \textbf{(8)}$$

$$[Ab]_o = [Ab] + [AbAg]^* \quad \textbf{(9)}$$

where $[Ab]_o$ is the total number of available binding sites and *[Ab]* is the number of unbound binding sites.

$$[AbAg]^* = \frac{K_a[Ab]_o[Ag]}{1 + K_a[Ag]} \quad \textbf{(10)}$$

Other adsorption isotherms based on the Langmuir isotherm such as the Sips isotherm (Langmuir-Freundlich isotherm) have also been used to describe the equilibrium binding kinetics of antibody-antigen in both solution and on the surface [76,77]. The Sips isotherm is similar to the Langmuir isotherm but it assumes that the adsorption sites have energies ranging from 0 to ∞. It is given by:

$$AbAg^{*} = \frac{[Ab_o]\{K_a[Ag]\}^s}{1+\{K_a[Ag]\}^s} \quad \textbf{(11)}$$

The index *s* is a measure of the surface heterogeneity of the adsorbed antibody. When antibodies are immobilized onto a substrate, some of them lose their functionality and thus the layer is heterogeneous with respect to the antigen binding ability. The low concentration limit of the adsorption isotherm (at low antigen concentrations) is dependent on the high affinity tail of the affinity distribution. The parameter *s* is a measure of how quickly the affinity tail decays. When *s* > 1, the tail decays rapidly and the adsorption follows the Langmuir isotherm. But when the value of *s* < 1, the tail of the affinity distribution curve decays slowly and the distribution of the antibodies which are capable of binding the antigen is spaced farther out. The value of *s* = 1, is the crossover point beyond which Langmuir Isotherm is sufficient to describe the binding between the antibody and antigen.

The amount of antigen adsorbed is evaluated for different concentration of the antigen in solution and the double reciprocal plot of equation 10 gives us a straight line with slope = $\frac{1}{[Ab_o]K_a}$ and intercept = $\frac{1}{[Ab_o]}$. For the Sips isotherm (equation 11), the curve was fitted to three parameters $[Ab_o]$, K_a and *s* using nonlinear regression in MATLAB's curve fitting tool box. In the following section, the results of the three immobilization strategies are discussed in detail.

Direct covalent immobilization

Figure 6a shows the resonant frequency change with time (blue curve) when Antimouse IgG (antigen), of concentration 60 nM binds to Mouse IgG (antibody) immobilized randomly by amine chemistry. The sharp frequency decrease initially shows the high binding affinity of Antimouse IgG to Mouse IgG present on the surface and the slower binding after the initial period shows that the binding is controlled by the equilibrium between Antimouse IgG in the solution and Antimouse IgG adsorbed on the surface. The large reservoir of Antimouse IgG solution is recycled and thus, this concentration of the solution can be assumed to be the concentration of the Antimouse IgG at equilibrium. The amount of antigen bound to the surface is directly proportional to the frequency decrease and is evaluated by the Sauerbrey equation (Equation 4) and a real time plot of amount of antigen adsorbed (Antimouse IgG) is shown in **Figure 6a** (black curve). The amount adsorbed is calculated for solution antigen concentrations ranging from 1 nM to 100 nM and fitted to the Langmuir (**Figure 7a**) and Sips adsorption isotherm (**Figure 7b**). The solid lines represent the curve fitted to the average values (from three experiments) of $[Ab_o]$ and K_a and individual data points are plotted on this curve with the error bars representing the standard error. The average values of $[Ab_o]$ and K_a evaluated from the Langmuir isotherm and Sips isotherm are presented in **Table 3** and **Table 4**. The degree of heterogeneity of the adsorbed antigen layer can be assessed by the parameter s in the Sips isotherm and is found to be 0.75 ± 0.04 which indicates that the antibody immobilized onto the surface is highly heterogeneous due to its random orientation.

Immobilization via Protein A

Figure 6b shows the resonant frequency change (blue curve) for the antibody (Mouse IgG) binding to Protein A on the crystal surface with time. The second marked decrease in **Figure 6b** is when, after saturating the surface with the antibody, antigen of concentration 100 nM is allowed to bind to the antibody. A real time plot of mass adsorbed is presented (black curve), from which the amount of antigen adsorbed on the surface can be evaluated. The amount of antigen adsorbed is evaluated for solution antigen concentrations ranging from 1 nM to 100 nM and is fitted to the Langmuir and Sips adsorption isotherm. $[Ab_o]$ and K_a are evaluated for both adsorption isotherms as discussed before and are presented in **Table 3** and **Table 4**. The heterogeneity of the adsorbed antibody (s) is greater than 1 showing that this scheme of immobilization is highly ordered.

Immobilization via biotinylated antibody on a streptavidin coated surface.

Figure 6c shows the frequency decrease (blue curve) for the binding of streptavidin, biotinylated antibody and antigen, of concentration 40 nM respectively. The mass adsorbed in each case is calculated using the Sauerbrey equation and the mass deposited is plotted with time (black curve). The data for amount of antigen adsorbed on the surface is evaluated for solution antigen concentrations ranging from 1 nM to 120 nM and as before, the $[Ab_o]$ and K_a are calculated using the Langmuir (**Table 3**) and Sips (**Table 4**) adsorption isotherm and $s>1$ represents a highly homogeneous surface.

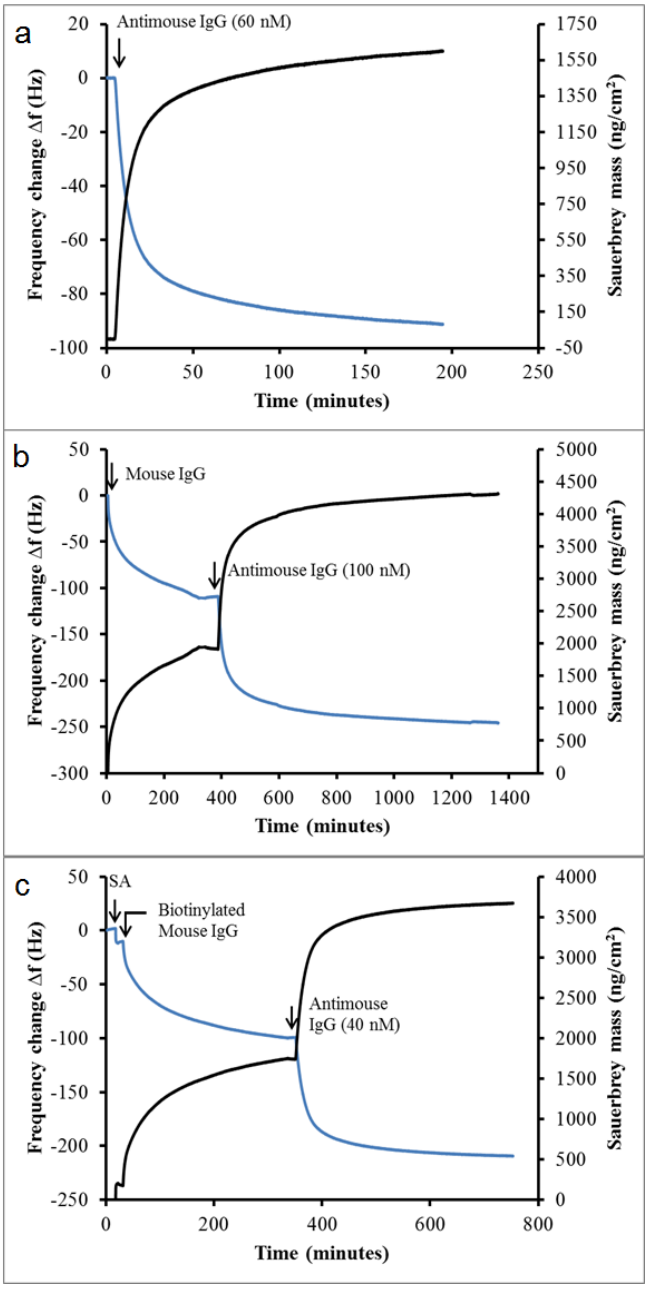

Figure 6. a) Direct covalent immobilization: Plot of frequency change (blue curve) and Sauerbrey mass calculated for the 5th overtone (black curve) with time for the adsorption of Antimouse IgG. **b)** Via Protein A: Plot of frequency change (blue curve) and Sauerbrey mass calculated for the 5th overtone (black curve) with time for the adsorption of Mouse IgG and subsequently, Antimouse IgG. **c)** Via biotinylated antibody: Plot of frequency change (blue curve) and Sauerbrey mass calculated for the 5th overtone (black curve) with time for the adsorption of streptavidin, biotinylated Mouse IgG and Antimouse IgG.

Table 3. Summary of results for the three immobilization chemistries for Langmuir adsorption isotherm. The average values for three experiments of [Ab_o] and K_a are presented here with the standard error.

LANGMUIR ADSORPTION ISOTHERM		
Immobilization method	**[Ab_o] (ng/cm^2)**	**K_a (*10^8) (1/M)**
Direct covalent immobilization	1726 ± 18	3.71 ± 0.20
Immobilization via Protein A	2683 ± 58	0.62 ± 0.01
Immobilization via biotinylated antibody	2120 ± 34	2.68 ± 0.13

Table 4. Summary of results for the three immobilization chemistries for Sips adsorption isotherm. The average values for three experiments of [Ab_o], K_a and s are presented here with the standard error.

SIPS ADSORPTION ISOTHERM			
Immobilization method	**[Ab_o] (ng/cm^2)**	**K_a (*10^8) (1/M)**	***s***
Direct covalent immobilization	1846 ± 36	3.11 ± 0.31	0.75 ± 0.04
Immobilization via Protein A	2621 ± 74	0.73 ± 0.02	1.25 ± 0.01
Immobilization via biotinylated antibody	2040 ± 23	2.69 ± 0.12	1.33 ± 0.09

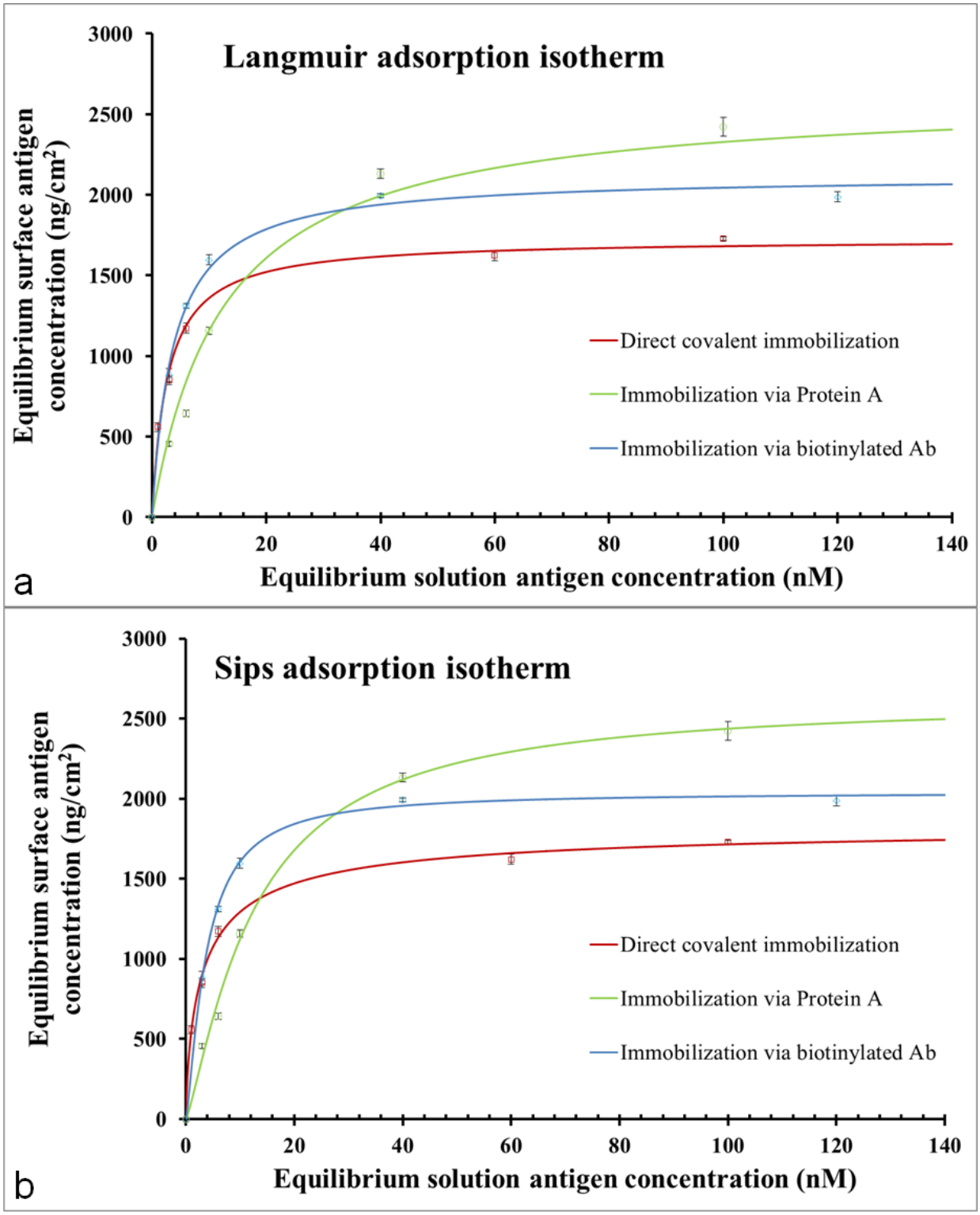

Figure 7. a) Langmuir adsorption isotherm and the **b)** Sips adsorption isotherm for all three immobilization schemes.

3.2.4 Conclusions

Two major inferences can be drawn from the equilibrium adsorption data fitted to the adsorption isotherms. Firstly, we can see that when the antibody is immobilized onto the quartz crystal surface directly using amine chemistry, the total surface concentration of active immobilized antibody, [Ab_o] is the lowest. This is expected when the antibodies are immobilized randomly, due to which they do not possess a favorable orientation to bind the antigen. [Ab_o] is the highest for immobilization via Protein A, as the antibodies have their antigen binding domains free and most of them have a favorable orientation to bind the antigen. Immobilization via biotinylated antibodies on a streptavidin coated surface is the most oriented scheme, but does not give the highest [Ab_o] probably due to excessive chemical modification of the antibody during biotinylation, which may have denatured the antibody.

Secondly, K_a which represents how much of the unbound active antibodies are able to form the antibody-antigen complex at equilibrium is the highest for random covalent immobilization. This is because although [Ab_o] is lower than the other schemes, the ones which are indeed active, are able to bind the antigen to a high degree due to lower steric hindrance offered by the antibodies to antigen binding as compared to the other schemes. Even though [Ab_o] for immobilization via Protein A is the largest, steric hindrance prevents the antigen from binding to the antibody on the surface and therefore has the lowest value of K_a.

The association equilibrium constant dominates over the total available binding sites at lower antigen concentrations, whereas nearing saturation, the total amount of available binding sites [Ab_o] becomes important. This is evident from **Figure 7a** and **Figure 7b**, where at low solution antigen concentrations of about 3 nM, the amount of antigen bound to the surface via Protein A is less than half than the other two methods. At intermediate antigen concentrations of around 18 nM for the Langmuir isotherm and 14 nM for the Sips isotherm, the amount of antigen

bound by direct covalent immobilization and immobilization via Protein A is equal but lesser than the amount bound by the biotinylated labeled antibody. At concentrations nearing the saturation concentration of the antigen, we see that immobilization of the Mouse IgG antibody by Protein A binds the highest amount of antigen. Therefore, at higher concentrations the random orientation of the antibodies immobilized by direct covalent immobilization gives rise to a large number of inactive antibodies on the surface which is not capable of binding the antigen. Immobilization of antibody using Protein A gives the maximum amount of active antibodies on the surface as Protein A has a natural affinity to the Fc region of antibodies which does not adversely affect the antibody's antigen binding ability. Although Protein A is immobilized randomly on the surface using direct covalent chemistry, it still gives the highest amount of active antibodies on the crystal surface at saturation. In reality, the most oriented scheme of immobilization investigated here is the biotinylated antibody which binds to an ordered layer of streptavidin which is in turn bound to an ordered self assembled monolayer of biotin thiol. Yet, the antibodies immobilized this way do not give the highest amount of antigen binding at saturation concentrations of the antigen which may be due to the excessive chemical modification of the antibody to label it with biotin. Therefore, when considering the choice for the immobilization scheme, the antigen or target molecule's concentration range becomes essential. At low concentrations, where the K_a dominates the antibody-antigen binding, direct covalent immobilization is adequate, whereas at higher antigen concentrations, $[Ab_o]$ dominates the equilibrium binding and an oriented immobilization scheme performs better.

3.3 RAPID POINT-OF-CARE DETECTION OF INFECTIOUS DISEASES USING LATERAL FLOW TECHNOLOGY

3.3.1 Introduction

Escherichia coli (*E. coli*) are one of the main components of the normal bacterial flora of the large intestine of mammals[78,79]. However, *E. coli* also may be the causative agent of several extra-intestinal infections besides the more common intestinal infections, such as travelers' diarrhea and hemorrhagic diarrhea [80-82]. Amongst the various extra-intestinal infections, *E. coli* is the most common cause of urinary tract infections (UTI) as well as several life threatening conditions including neonatal meningitis and sepsis [83,84].

Shiga toxigenic *E. coli* are bacteria responsible for severe gastrointestinal infections in humans. There are certain strains which are more virulent than others, for example, the STX-1 and STX-2 strains. Furthermore, a combination of the two strains is known to cause greater harm leading to cases of hemolytic-uremic syndrome (HUS) and thrombotic thrombocytopenic purpura [85,86]. Large outbreaks of gastrointestinal disease caused by these strains and their high mortality rates in developing countries have placed their timely detection and diagnosis high on the priority list for communicable diseases.

Klebsiella pneumoniae (*K. pneumoniae*) is another gram negative bacterium which is present in the colon. It is second leading cause of UTI and is responsible for a number of other infections such as pneumonia, septicemia and neonatal sepsis [87,88] . *Klebsiella pneumoniae*, the most important *Klebsiella* species is an opportunistic pathogen which causes infections associated with hospitalization. Immuno-compromised individuals are more susceptible to *K. pneumoniae* infections and the high mortality rates and the surge of antibiotic resistant strains have renewed interest in the rapid early diagnosis of *K. pneumoniae.*

Currently, diagnosis of most extra-intestinal infections caused by bacteria including *E. coli* is made by bacterial culture which often takes at least 24-48 hours. Newer DNA amplification based techniques like PCR can give results much faster but are not widely used for diagnosis of bacterial infection, in part because they require considerable operator skill and expensive equipment. Recently, a novel, specific, and rapid technique for amplification of DNA under isothermal conditions has been reported [89,90]. This technique, termed Loop mediated isothermal amplification (LAMP) requires a constant temperature condition throughout the reaction, ranging from 62-66 ^{o}C for a period of 30-60 minutes. Thus, LAMP can be conducted on a simple heating block, obviating the need for an expensive thermal cycling machine such as required for PCR. In this study, we developed and characterized LAMP primers and amplification protocols for *E. coli mal*B, *E. coli STX-1 and K. pneumoniae*. The amplification products can be detected visually by observing the fluorescence upon addition of a DNA intercalating dye such as Eva Green, Sybr Green, Ethidium Bromide or Propidium Iodide [91]. The appearance of turbidity has also been made use for detection of the amplified product [92]. More recently, DNA based lateral flow assays in which two small molecule labels, one which binds to reporter particles and the other which binds to the nitrocellulose membrane are made use of in a sandwich type format after amplification by LAMP [93-96]. Lateral flow strips offer a low-cost, sensitive and instrumentation free detection method. We report the details of LAMP amplification of *E. coli mal*B, *E. coli STX-1* gene and *K. pneumoniae citw* along with the detection on lateral flow strips using a set of anonymized human biological specimens. Multiplexing detection of two organisms has also been successfully demonstrated. The results of the LAMP/Lateral flow detection were compared with PCR as well as bacterial culture results.

3.3.2 Detection on lateral flow strips

A typical lateral flow strip consists of a porous membrane usually made of nitrocellulose, sample and absorbent pads assembled on an adhesive backing strip which provides structural integrity to the membrane along with the other components. Sometimes, a conjugate pad is also included on which the reporter particles are deposited. Colloidal gold nanoparticles (15-80 nm) are the most commonly used reporter particles due to their optical properties in the nanometer scale and the ease of functionalizing the surface with antibodies and other biomolecules such as DNA and RNA. Other particles such as latex [97], carbon black [98,99], liposomes [100,101] and Up-Converting Phosphur (UCP) [102] have also been used in lateral flow assays. Initially, detection was carried out using enzymatic labels such as in ELISA [103], but now, reporter particles such as the ones mentioned above offer higher stability than the enzymatic labels. The sample pad helps to draw the sample solution on to the nitrocellulose membrane and the absorbent pad helps to wick the sample and the reporter particles towards the end of the strip. In a typical sandwich type immunoassay, the target sample is allowed to bind to the reporter particles in the presence of a flow buffer and travels along the membrane via the action of capillary forces. If the target is present in the sample, the reporter particle-target complex binds to the test line making possible for visual detection in the case of gold nanoparticles or detection via a detector. Sometimes, the remaining reporter particles which do not bind the test line travel further downstream to bind to the control line, to which the reporter particles bind directly.

3.3.2.1 Principle of detection of amplified DNA on lateral flow strips

The DNA amplified either by PCR or LAMP must contains two labels, which in the case of *E. coli mal*B is chosen to be FITC and biotin and for *E. coli STX-1* and *K. pneumoniae* is chosen to be Digoxigenin and biotin (**Figure 8a**). This is mixed with the GNPs conjugated with streptavidin (**Figure 8b**) to which the biotin label on the amplified DNA binds (**Figure 8c**). The DNA-GNP complex is applied to the sample pad and is flowed onto the membrane. The FITC label on the amplified *E. coli mal*B DNA binds to the Anti-FITC antibody on the membrane and the *E. col mal*B-GNP complex aggregate at the test line (**Figure 8d**). Thus, for a successful positive assay to be detected visually, a two layer sandwich structure, namely the binding between biotin present on the DNA to streptavidin on the GNPs and FITC on the DNA with Mouse Anti-FITC on the membrane is needed. The unbound GNPs which are conjugated with streptavidin directly bind to a secondary antibody (Anti-streptavidin) present on the control line. The aggregation of the colloidal gold on the control line shows that the streptavidin present on the GNPs is capable of binding. If the control line is not bound by the GNPs, the assay must be disregarded as the cause for a negative test line and control line could be due to the denaturing of the streptavidin rather than the absence of target DNA in the sample solution. Similarly for the case of *E. coli STX-1* and *K. pneumoniae,* a two layer sandwich structure between the biotin label to streptavidin on the GNPs and the Dig label on the amplified DNA to the Anti-Dig antibody on the membrane is required.

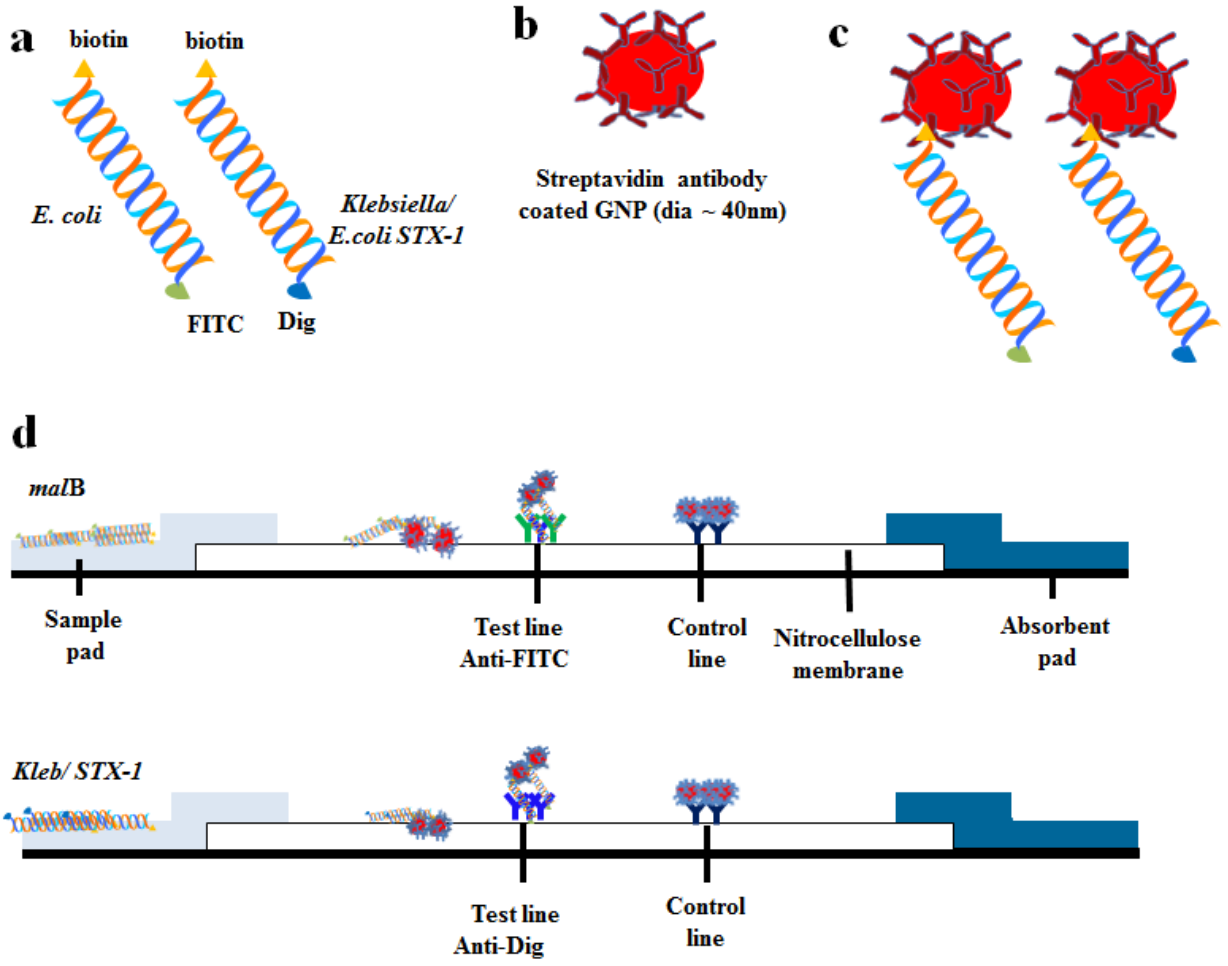

Figure 8. Schematic of binding events on a lateral flow strip for labeled amplified DNA detection **a)** FITC (green) and Biotin (yellow) labeled amplified *E. coli mal*B dsDNA and Digoxigenin (blue) and Biotin (yellow) labeled amplified *E. coli STX-1/K. pneumoniae*. **b)** Schematic of streptavidin coated GNP. **c)** Streptavidin coated GNP binds to the Biotin label on the amplified DNA product. **d)** Schematic of a positive test for *E. coli mal*B (top) and *E. coli STX-1/K. pneumoniae* (bottom).

3.3.2.2 Preparation of lateral flow strips

We have investigated four different lateral flow strip nitrocellulose membranes which are shown in **Table 5** with their properties.

Table 5. List of nitrocellulose membranes. (Capillary rise is measured as the time taken to wet 4 cm of the membrane.)

Sl no	Manufacturer	Description	Capillary rise sec/4 cm	Thickness (μm)	Backed
1	Whatman membranes	AE 98	160--210	120	No
2	Whatman membranes	AE 99	120--160	120	No
3	Whatman membranes	FF 125	100--150	200	Mylar
4	Pall Corporation	VIVID170LFNC	150-225	200	Polystyrene

The first two membranes are unbacked with just the nitrocellulose membrane. The last two are backed membranes which are backed with Mylar and polystyrene respectively. Unbacked membranes are typically used in preliminary work where the concentration of the antibodies, pH and the amount of target needs to be optimized. They are difficult to handle owing to their brittle nature as compared to backed membranes which offer greater robustness. The lateral flow strips were made by assembling the nitrocellulose membrane, the glass fiber sample pad (FUSION 5, Whatman GE Healthcare), and the absorbent pad (CF5, Whatman GE Healthcare) on a polystyrene adhesive backing strip (G&L Precision Die Cutting, LLC).

To detect the labeled amplified PCR or LAMP product the nitrocellulose membrane is striped across its width with Anti-FITC (for *E. coli mal*B) or Anti-Dig antibody (for *E. coli STX-1 and K. pneumoniae*) (Sigma Aldrich) of concentration 1 mg/mL in the striping buffer (PBS, pH

7.4), which constitutes the test line and Anti-streptavidin IgG (Sigma Aldrich) of concentration 1 mg/mL in the striping buffer which constitutes the control line. Approximately, 1000 ng of Anti-FITC/Anti-Dig antibody and 720 ng of Anti-streptavidin were dispensed using an airbrush (Iwata HP-A Plus) and the lines were striped at a distance of 30 mm apart from each other. The strips were dried at room temperature for 1 hour before use and were stored in air-tight containers at room temperature.

Detection procedure

The colloidal gold nanoparticles (GNPs) conjugated with streptavidin purchased from Bioassay Works® have a mean diameter of 40 nm and a concentration of 15 OD. About 10 μL of the PCR product was added to 10 μL of the GNPs in 200 μL of the flow buffer. This was then applied to the sample pad of the lateral flow strip and was allowed to develop for 25 minutes. The strip was again washed with the flow buffer to remove any GNPs which were bound to the membrane non-specifically.

Effect of pH

Three different buffers were used, namely HEPES (pH 6.3), PBS (pH 7.3) and Tris-HCl (pH 8.8) as the flow buffers for the lateral flow assay. At higher pH, when the Tris-HCl buffer was used as the flow buffer, the binding was almost non-existent. We found that the HEPES buffer which consists of HEPES (10 mmol), NaCl (135 mmol), BSA (2%) and Tween 20 (0.05%) performed best for our assay (results not shown) as was used as the lateral flow buffer for all future experiments.

3.3.3 Detection of PCR product on lateral flow strips

The forward primer and reverse primers for *E. coli mal*B were labeled with FITC and biotin respectively. For both *E. coli STX-1* and *K. pneumoniae*, the forward primer and reverse primers were labeled with Digoxigenin and biotin respectively. These forward and reverse primers were used as the outer primers (F3 and B3) for LAMP as will be seen later. **Table 6** shows the sequence of the primers used and **Figure 9** shows their location on the genome.

Table 6. PCR primers for *E. coli mal*B, *E. coli STX-1* and *K. pneumoniae.*

Organism	Primer name	Primer Sequence
*E. coli mal*B	F3	5'-FITC-ATTTACCGCAGCCAGACG -3
*E. coli mal*B	B3	5'-Bio-GCCATCTCCTGATGACGC-3'
E. coli STX-1	F3	5'-Dig-ACAGAGGGGATTTCGTAC-3'
E. coli STX-1	B3	5'-Bio-GATGACAATTCAGTATTAATGC-3'
K. pneumoniae	F3	5'-Dig-AAACTGATTGGTCTGCCGG-3'
K. pneumoniae	B3	5'-Bio-TGCATCCCTATCTTTTTACC-3'

***E. coli malB* gene (GDB J01648)**

```
1      GAAACACCAT ACCAACGCCA CGTTCTGCTG GCGGAGTGTC ATTCATCCGT TTCTCACCGA

61     TGAACAGGTC GCCGCTGGTG ATCGTCTCAA GCCCGGCAAT CATGCGCAGT AAAGTCGATT
          F3
121    TACCGCAGCC AGACGGTCCG ACAAACACCA CGAATTCACC TTCATGGATA TCGAGATTGA

181    TATCTTTCGA TACCACGACC TCGCCCCAGG CTTTCGTTAC ATTTTGCAGC TGTACGCTCG

241    CCATGCCCTT CTCCCTTTGT AACAACCTGT CATCGACAGC AACATTCATG ATGGGCTGAC


301    TATGCGTCAT CAGGAGATGG CTTAAATCCT CCACCCCCTA GCTTTTTTAT GGGGGAGGAG
                  B3
```

***E. coli STX-1 gene* (GDB: AM230663.1)**

```
                       F3
1      TTTTCGGCAA ATACAGAGGG GATTTCGTAC AACACTGGAT GATCTCAGTG GGCGTTCTTA

61     TGTAATGACT GCTGAAGATG TTGATCTTAC ATTGAACTGG GGAAGGTTGA GTAGTGTCCT

121    GCCTGATTAT CATGGACAAG A-CTCTGTTC GTGTAGGAAG AATTTCTTTT GGAAGCATTA

181    ATGCAATTCT GGGAAGCGTG GCATTAATAC TGAATTGTCA TCATCATGCA TCGCGAGTTG

241    CCAGAATGGC                                B3
```

***K. pneumoniae* (GDB AF411142)**

```
1      GGGACCCTCG CCTCCGGCGC GCTGCTGGCG GTACTGCTGT ATATGATGGG GATGCTCGGC

             F3
61     CACAAACTGA TTGGTCTGCC GGCGCCGGTA GGCATGCTGT TCCTCGCGGT ACTGTTAAAG

121    CTGGCTAACG TGGTGTCTCC GCGTCTGCAG GAGGGGTCGC AGATGGTGTA TAAATTCTTC

181    CGCACCGCGG TCACCTACCC GATCCTCTTT GCCGTCGGCG TGGCGATCAC TCCGTGGCAG


                                        B3
241    GAACTGGTAA ACGCCTTCAC TTTAACCAAC CTGCTGGTGA TCGTCAGTAC CGTCTCCGCG
```

Figure 9. Location of the PCR primers on the *E. coli malB* (GDB J01648), *E. coli STX-1* (GDB AM230663.1) and *K. pneumoniae* (GDB AF411142) gene respectively.

PCR reaction

The PCR reaction mixture (total 25 μL) contains 1 μL each of the labeled forward and reverse primers (concentration 10 μM), 0.8 μL of Taq DNA polymerase, Thermopol reaction buffer (1X) which contains 20 mM Tris –HCl (pH 8.8, @ 25ºC), 10 mM KCl , 10 mM $(NH_2)SO_4$, 2 mM $MgSO_4$, 0.1% Triton X-100 (New England Biolabs Inc., MA, USA) and 2 μL of 1.25 mM dNTP. The PCR reaction was conducted in a BioRAD PCR thermocycler with 40 or 15 temperature cycles of 95 ^{o}C for 30 seconds, 57 ^{o}C for 30 seconds and 72 ^{o}C for 90 seconds.

Detection of PCR products on agarose gel

The PCR amplified *E. coli mal*B, *E. coli STX-1* and *K. pneumoniae* were detected in a 2% agarose gel with Sybr DNA staining dye with UV illumination along with the negative target control (NTC). Comparison with the ladder shows (**Figure 10**) that the band for the PCR amplified *E. coli mal*B corresponds to 195 bases, *E. coli STX-1* to 210 bases and *K. pneumoniae* corresponds to 222 bases which is the region between the forward primer F3 and the reverse primer B3.

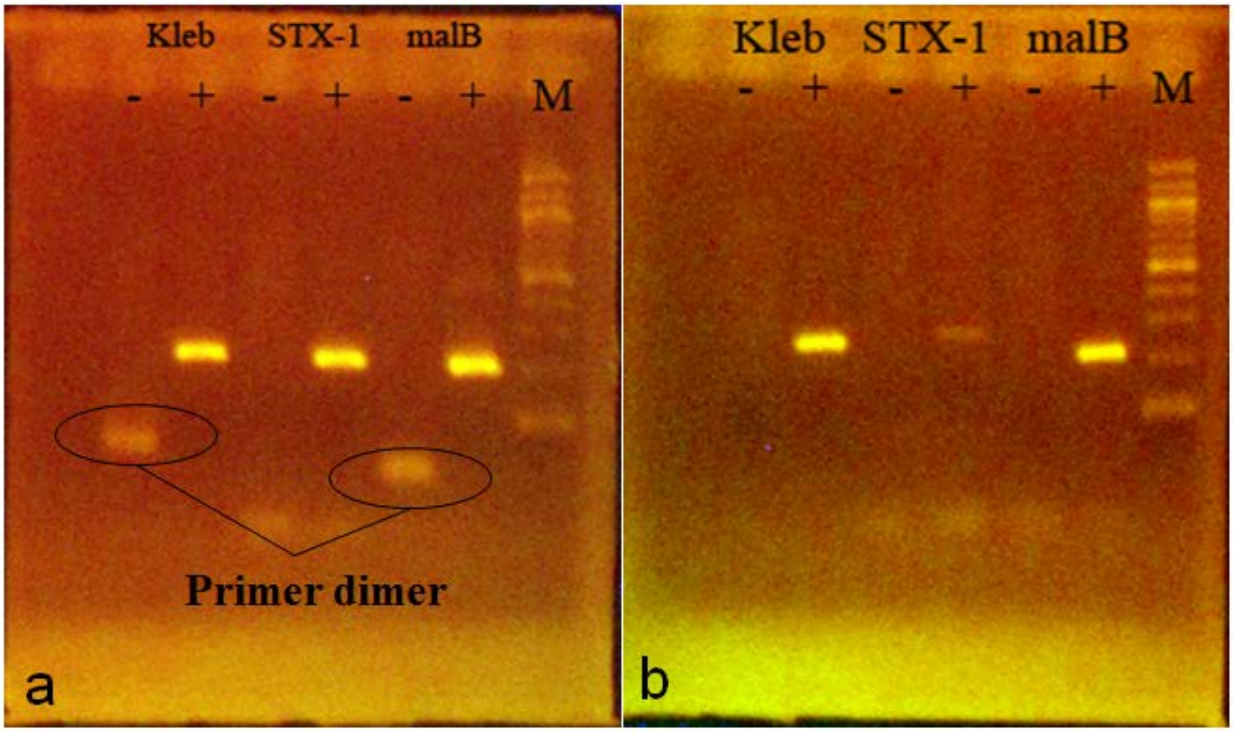

Figure 10. Gel image of *K. pneumoniae, E. coli STX-1* and *E. coli mal*B, amplified by PCR for **a)** 40 cycles and **b)** 15 cycles with the negative target control (NTC) on the left followed by the band indicating positive amplification and the ladder (M). The 100kb ladder shows that the amplified product is about 200 bps long. For the 40 temperature cycles, the formation of primer dimer is visible (shown in the black circles) whereas for 15 cycles, no primer dimer seems to be present. The target used for PCR was the *K. pneumoniae* clone, *E. coli STX-1* DNA extracted from urine samples and *E. coli mal*B clone. As the copy number of the clone is very high (of the order of 10^6 copies/µL), even at 15 cycles there is a strong positive band for *K. pneumoniae* and *E. coli mal*B, whereas for the extracted *E. coli STX-1* DNA, it is only faintly visible.

Detection on lateral flow strips

Shown in **Figure 11** is the detection of *E. coli mal*B after 40 cycles with its negative target control (NTC) on all four lateral flow membranes mentioned before. As can be seen, the NTC also shows a faint binding which is due to the formation of primer-dimer. In PCR the primary interaction is between the primers and the template/target which gives rise to specific amplification. However, as the concentration of the forward and reverse primers is high, weak primer interaction with each other cause the formation of non-specific dsDNA products which reduce the amplification efficiency. Studies have shown that even no base complementarity at the 3` end causes a primer dimer to be formed after 40 cycles [104]. Although this has an effect on the efficiency of the amplification, in most cases it is not deleterious to the performance of PCR. When labeled PCR products are run over a nitrocellulose membrane in a lateral flow strip, the only labels that need to be detected are the labels on the specifically amplified product. So, when two labeled primers form dimers, it leads to the formation of a short dsDNA product which is non-specific, but one which contains both labels. This labeled non-specific product acts as the labeled specifically amplified product and produces a false positive as seen in **Figure 11**. The formation of primer dimers can be reduced by careful primer design, reduction in the number of cycles for amplification, hot start PCR, touch-down PCR and other methods. When PCR for *E. coli mal*B was carried out for 15 cycles, there is no primer dimer seen in the gel and there is no false positive as seen in **Figure 12**. The backed membranes namely VIVID170, Pall and FF125, Whatman had better sensitivity and contrast between the positive and the negative samples when compared to the unbacked membranes. FF125 was chosen to be the membrane as it had excellent flow properties and high sensitivity and was used thereafter. **Figure 13** shows the detection of *E. coli STX-1* and *K. pneumoniae* amplified by PCR for 15 cycles on lateral flow strips assembled with FF125 membranes. Here the test line was Anti-Dig antibody as previously mentioned.

To validate the formation of primer-dimer, real time PCR was performed in an Applied Biosystems 7900HT Real time PCR machine with 1 µL Sybr Green dye added to detect the real time fluorescence. Sybr Green is a DNA intercalating dye which binds specifically to dsDNA. So, if there is target present, the intensity of the fluorescence increases as the dsDNA is being synthesized. PCR was conducted with one positive control, where the *E. coli mal*B clone was added to the reaction as the target and one NTC where de-ionized water was added as the target. The primers used were the forward and reverse primers (F3 and B3) for *E. coli mal*B whose sequences are given in **Table 6**. After 40 temperature cycles of PCR at 95 ^{o}C for 30 sec, 57 ^{o}C for 30 sec and 72 ^{o}C for 1 min, the temperature is brought to 60 ^{o}C where it is maintained for 1 minute. The temperature is ramped up slowly at a rate of 2 ^{o}C/ min and the real time fluorescence intensity is recorded. At a particular temperature, the dsDNA products dissociate and this temperature is a function of the length of the dsDNA. If there is any primer dimer present, the temperature at which the dimers dissociate would be lesser than the specifically amplified positive control. The dissociation curve plots the derivative of the fluorescence intensity change versus temperature which gives information about the dissociation temperature of the primer-dimer (from the NTC), if present, and the amplified product. From **Figure 14** it can be observed that for the positive control PCR reaction, the dissociation temperature is around 84 ^{o}C and for the NTC it is around 73 ^{o}C. The primers would therefore have to be redesigned or the number of cycles has to be reduced to around 15 which would have a negative effect on the sensitivity.

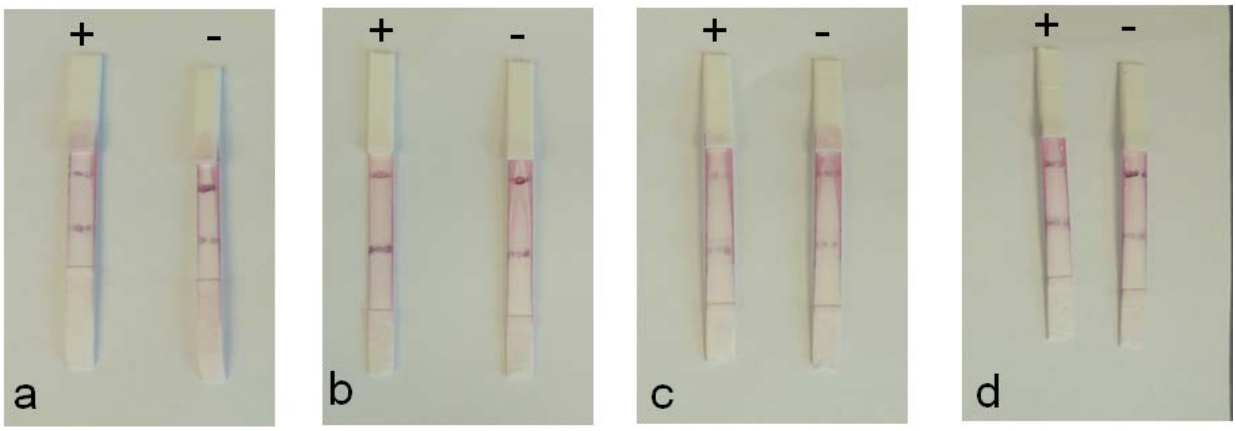

Figure 11. Detection of PCR amplified *E. coli mal*B DNA labeled with FITC and biotin after 40 cycles along with their NTCs (denoted by the '-' sign on the figure) on lateral flow strips assembled with different nitrocellulose membranes **a)** VIVID170LFNC, Pall Corp **b)** FF125, Whatman **c)** AE99, Whatman **d)** AE98, Whatman.

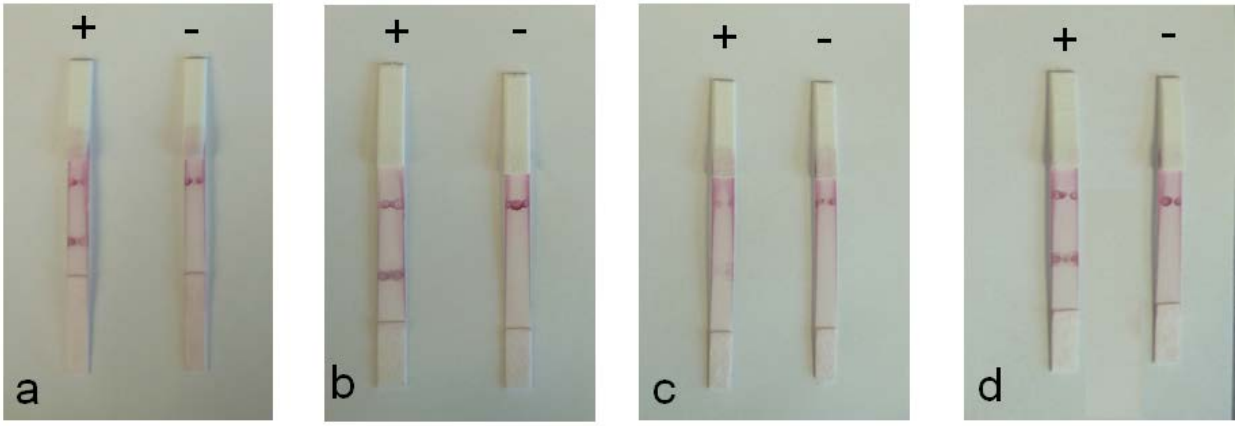

Figure 12. Detection of PCR amplified *E. coli mal*B DNA labeled with FITC and biotin after 15 cycles along with their NTCs (denoted by the '-' sign on the figure) on lateral flow strips assembled with different nitrocellulose membranes **a)** VIVID170LFNC, Pall Corp **b)** FF125, Whatman **c)** AE99, Whatman **d)** AE98, Whatman.

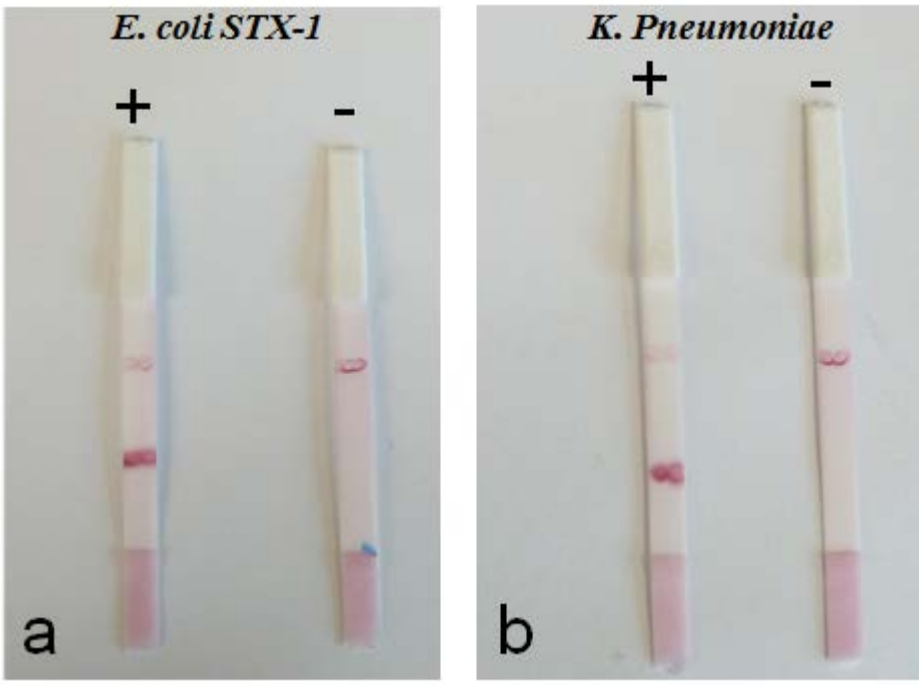

Figure 13. Detection of PCR amplified **a)** *E. coli STX-1* and **b)** *K. pneumoniae* DNA labeled with Dig and biotin after 15 cycles along with their NTCs (denoted by the '-' sign on the figure) on lateral flow strips assembled with FF125, Whatman.

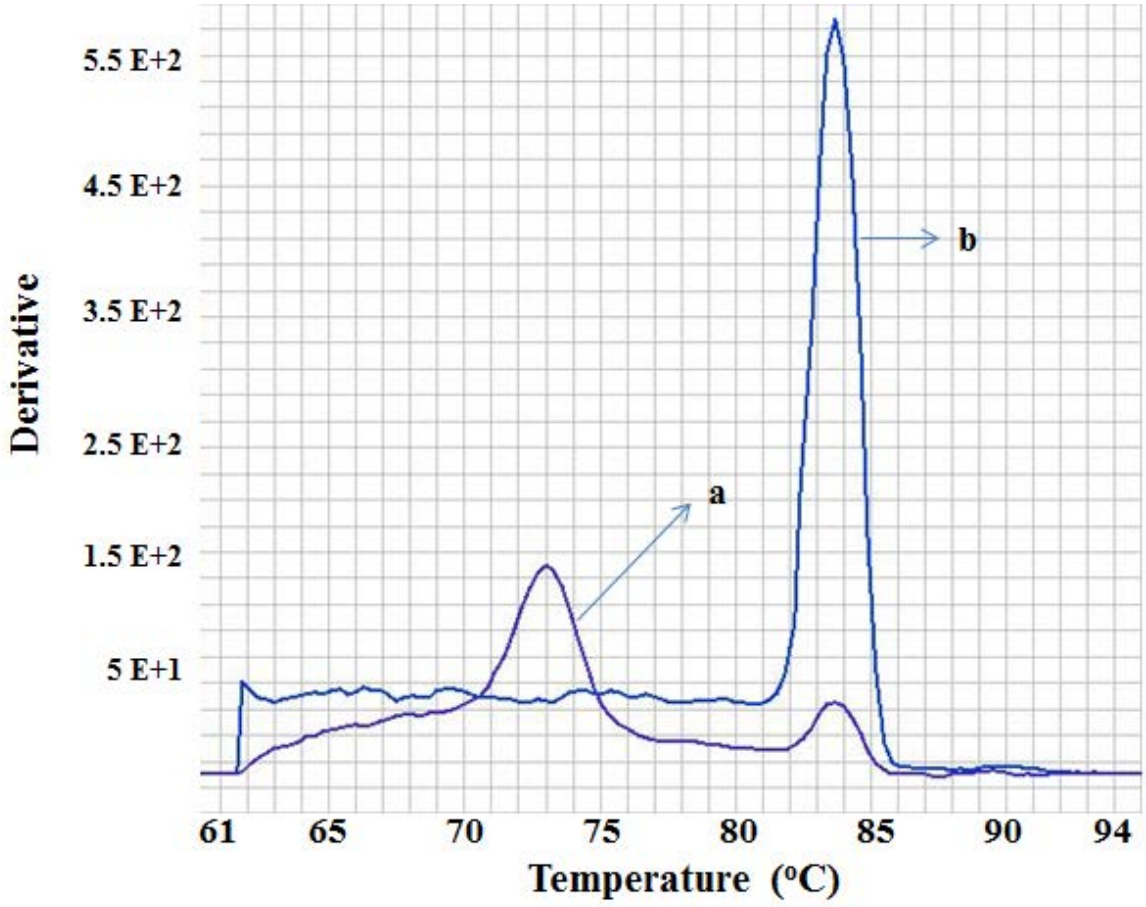

Figure 14. Dissociation curve for *E. coli mal*B amplification products after PCR for 40 cycles in a real time PCR machine. **a)** NTC **b)** Specifically amplified *E. coli mal*B positive control

The primers for PCR were redesigned for *E. coli mal*B by extending them to cover a region of 308 bps (See the location of F3 and B3 in **Figure 17**) and was checked again with real time PCR to see if any dimers were formed. Shown in **Figure 15** is the dissociation curve for the newly designed PCR primers which are compared alongside the old primers. As can be seen, there is no formation of primer dimer and this can now be used to amplify the *E. coli* target with 40 temperature cycles and then run on a lateral flow strip without encountering a false positive for the NTC.

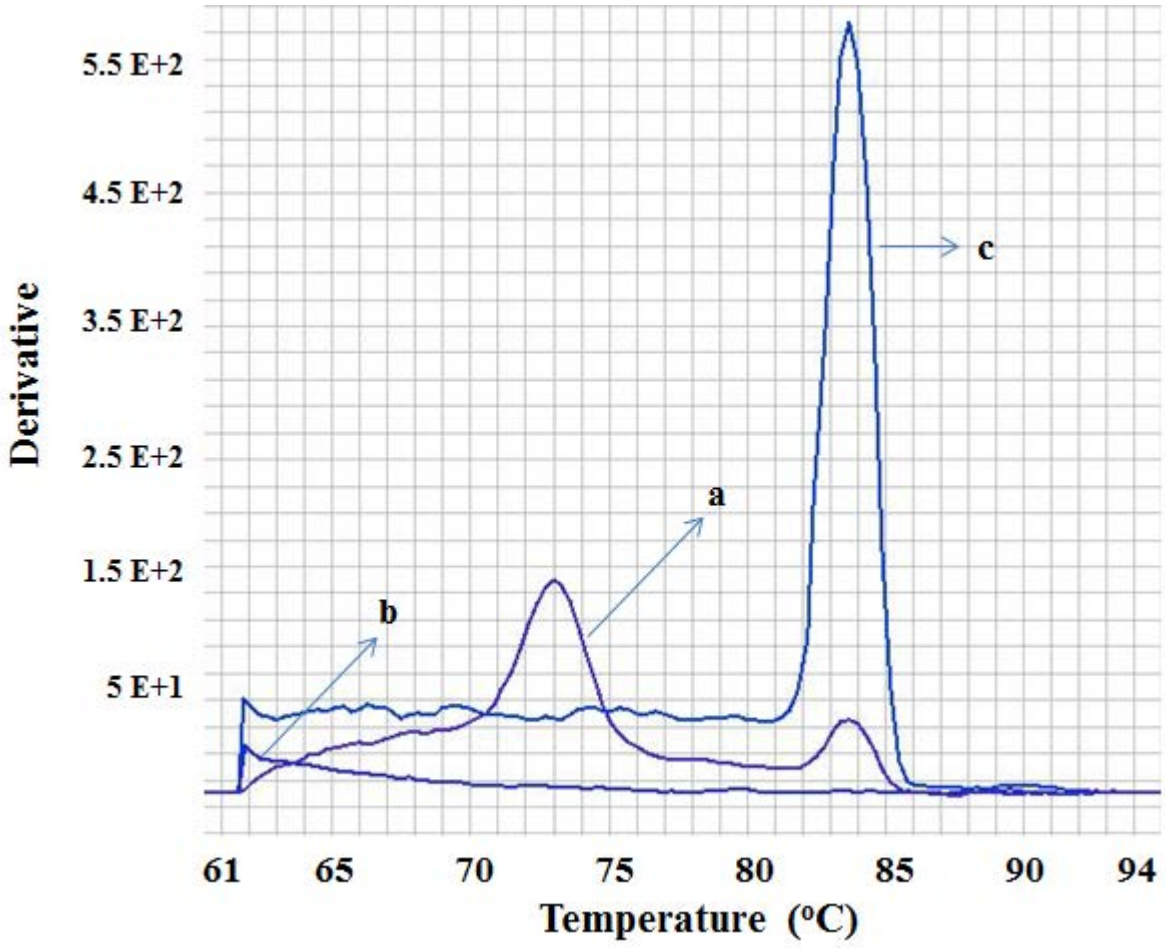

Figure 15. Dissociation curve for *E. coli mal*B amplification products after PCR for 40 cycles in a real time PCR machine. **a)** NTC with old primers **b)** NTC with the extended primers **c)** Specifically amplified *E. coli mal*B positive control

3.3.4 LAMP primer design

Nucleic acid amplification is the cornerstone for detection of genetic variation, infectious diseases and harmful mutations. PCR is the most widely used nucleic acid amplification technique, but recently other DNA amplification techniques such as NASBA (nucleic acid sequence based amplification), self-sustained sequence replication (3RS) and strand displacement amplification (SDA). Each of these above mentioned methods utilize a different technique to reinitiate the DNA replication process from the previous round. PCR utilizes heat denaturation, NASBA and 3RS utilize a set of transcription and reverse transcription to amplify and SDA and LAMP utilize the polymerase's strand displacement activity to amplify without heat denaturation of the DNA strands.

Although PCR thermal cyclers are expensive and require skilled personnel to work it, they are still the most reliable nucleic acid amplification technique available today. This is due to the fact that the other methods barring LAMP suffer from low specificity and residual coamplification of unwanted sequences which increase background noise. LAMP as first described by Notomi et al [89] is isothermal and relies on the heavy strand displacement activity of the *Bst* DNA polymerase enzyme. It can be carried out with 4 primers namely F3, B3 (outer primers) and FIP and BIP (inner primers). The addition of loop primers has been shown to accelerate the reaction [90] such that the total time required for amplification is about half the original time when only 4 primers are used. In the initial steps all four primers are used, but during the later stages, only the inner primers are used. Shown below in **Figure 16** is the location of the six distinct regions which are recognized by the LAMP primers:

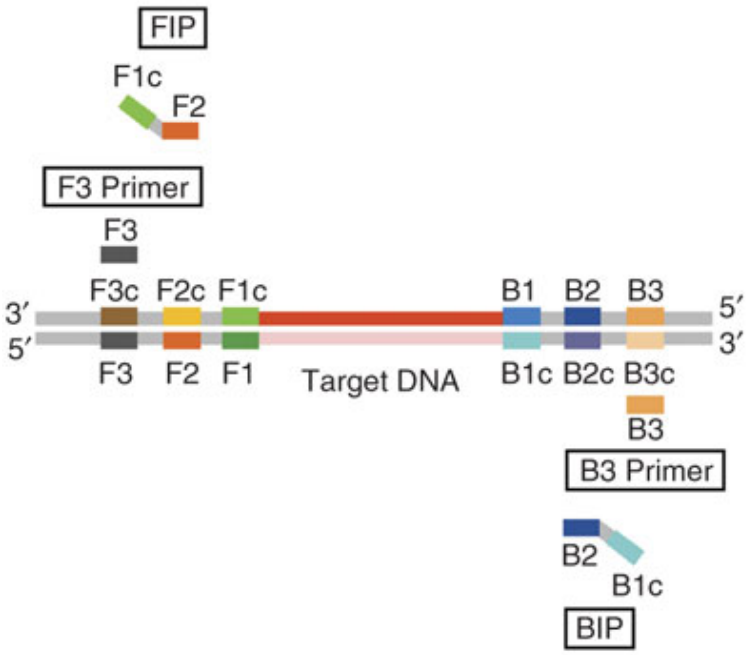

Figure 16. LAMP primers and their location on the target DNA.

The mechanism of LAMP amplification can be described in the following steps:

1. First, the F2 portion of FIP (F1c+F2) binds to the F2c region on the target DNA and completes the strand.
2. F3 binds to the F3c region and start to build the complementary strand while displacing the DNA strand formed by FIP with the help of the strand displacing *Bst* polymerase. Now, the displaced strand contains F1c, the region from the FIP primer which was unused in the building of the complementary strand and F1 which was synthesized. When this single strand DNA is broken off, a loop is formed by the binding of F1 and F1c.
3. The region B2 (B1c+B2) of BIP binds to the B2c region of this displaced ssDNA strand which contains the loop and the complementary strand is synthesized while opening out the loop formed between F1 and F1c.

4. B3 now binds to the B3c region and starts to build the complementary strand while displacing the DNA strand formed by BIP with the help of the strand displacing *Bst* polymerase. This gives rise to a ssDNA strand with two loops: One formed between F1 and F1c and the other formed between B1 and B1c.

   This serves as the starting material for LAMP amplification.

5. F2 of FIP (F1c+F2) now binds to the loop and DNA is synthesized. Thus, with a single strand DNA template, two identical strands complementary to the starting structure are synthesized. As the F1 portion of the loop elongates, it displaces the loop formed by the B1 + B1c. The new strand created by the F1 portion of the loop also contains B1c + B1 which forms a loop. With the newly synthesized strand by the F1 portion of the loop as the template, the loop continues to build displacing the F1c portion of the primer which started step 5 and also the strand which was synthesized by it. This strand displaced is again the starting material for LAMP.
6. The single looped (B1+B1c) dsDNA structure left behind now has BIP bind to it and carry out the building of the complementary strand. As the new complementary strand is being synthesized, the other strand which was complementary to the target before BIP binds to it gets displaced. This structure now has 3 loops. Simultaneously, the starting material which was formed in step 5 also has BIP bind to it and build its complementary strand.
7. The process continues and during amplification, a series of products are formed which are multiples of the region marked by F3 and B3. Thus when these amplification products are run in a gel, they give rise to a ladder like pattern instead of a single band as in PCR.

The LAMP primers for *E. coli mal*B, *E. coli STX-1* and *K. pneumoniae* were designed using Primer Explorer Primer Explorer V3 software provided by Eiken Chemical Co., Ltd, which can

be found here: http://loopamp.eiken.co.jp/e/lamp/primer.html. The primer sequences are given in **Table 7** and their location on their respective genome is as shown in **Figure 17**.

Table 7. LAMP primer sequences

E. coli malB gene

Primer	Sequence	Bases
F3	5'-CTGGTGATCGTCTCAAGCCCGGC-3'	23
B3	5'-GCCGCGTTCTCATCCTCCCG-3'	20
FIP (F1C+F2)	5'-CTGGGGCGAGGTCGTGGTAT-TCCGACAAACACCACGAATT -3'	42
BIP (B1c+B2)	5'-CATTTTGCAGCTGTACGCTCGC-AGCCCATCATGAATGTTGCT-3'	44
Loop F	5'-FITC- ATCAATCTCGATATCCATGAAGGTG-3'	25
Loop B	5'-Biotin-CTTTGTAACAACCTGTCATCGACA-3'	24

E. coli STX-1 gene

Primer	Sequence	Bases
F3	5'- ACAGAGGGGATTTCGTAC-3'	18
B3	5'- GATGACAATTCAGTATTAATGC-3'	22
FIP (F1c+F2)	5'-CCTTCCCCAGTTCAATGTAAG-CTGGATGATCTCAGTGGGC-3'	40
BIP (B1+B2c)	5'-GTCCATGATAATCAGGCAGG-GCATTAATGCAATTCTGGGAAG-3'	42
Loop F	5'- Dig-CATCTTCAGCAGTCATTAC-3'	19
Loop B	5'-Bio-CTGTTCGTGTAGGAAGAATTTC-3'	22

K. pneumoniae citw gene

Primer	Sequence	Bases
F3	5’-AAACTGATTGGTCTGCCGG-3’	19
B3	5’-GACGATCACCAGCAGGTTG-3’	19
FIP (F1c+F2)	5’-TACACCATCTGCGACCCCTC CTGTTCCTCGCGGTACTGT -3’	39
BIP (B1+B2c)	5’-GGCAAAGAGGATCGGGTAGGTGGGAACTGGTAA ACGCCTTCA-3’	42
Loop F	5’-Dig-ACACCACGTTAGCCAGCTT-3’	19
Loop B	5’-Biotin-CGTGGCGATCACTCCGT -3’	17

*E. coli mal*B gene (GDB J01648)

```
1     GAAACACCAT ACCAACGCCA CGTTCTGCTG GCGGAGTGTC ATTCATCCGT TTCTCACCGA

                                F3 ──────►
61    TGAACAGGTC GCCGCTGGTG ATCGTCTCAA GCCCGGCAAT CATGCGCAGT AAAGTCGATT

                                F2                                ◄──────  LF
121   TACCGCAGCC AGACGGTCCG ACAAACACCA CGAATT*CACC TTCATGGATA TCGAGATTGA

                                F1c                       B1c
181   TATCTTTCGA TACCACGACC TCGCCCCAGG CTTTCGTTAC ATTTTGCAGC TGTACGCTCG

                                LB ──────►          B2
241   CCATGCCCTT CTCCCTTTGT AACAACCTGT CATCGAC|A|GC AACATTCATG ATGGGCTGAC

301   TATGCGTCAT CAGGAGATGG CTTAAATCCT CCACCCCCTA GCTTTTTTAT GGGGGAGGAG

361   GCGGGAGGAT GAGAACGCGG CTTCTGTGA  389
          ◄──────  B3
```

E. coli STX-1 (GDB AM230663.1)

```
                      F3 ──────►                  F2
1     TTTTCGGCAA ATACAGAGGG GATTTCGTAC AACACTGGAT GATCTCAGTG GGCGTTCTTA

          ◄──────  LF                 F1c
61    TGTAATGACT GCTGAAGATG TTGATCTTAC ATTGAACTGG GGAAGGTTGA GTAGTGTCCT

            B1                  LB ──────►
121   GCCTGATTAT CATGGACAAG A-CTCTGTTC GTGTAGGAAG AATTTCTTTT GGAAGCATTA

        B2c
181   ATGCAATTCT GGGAAGCGTG GCATTAATAC TGAATTGTCA TCATCATGCA TCGCGAGTTG
                                ◄──────  B3
241   CCAGAATGGC
```

K. pneumoniae citw (GDB AF411142)

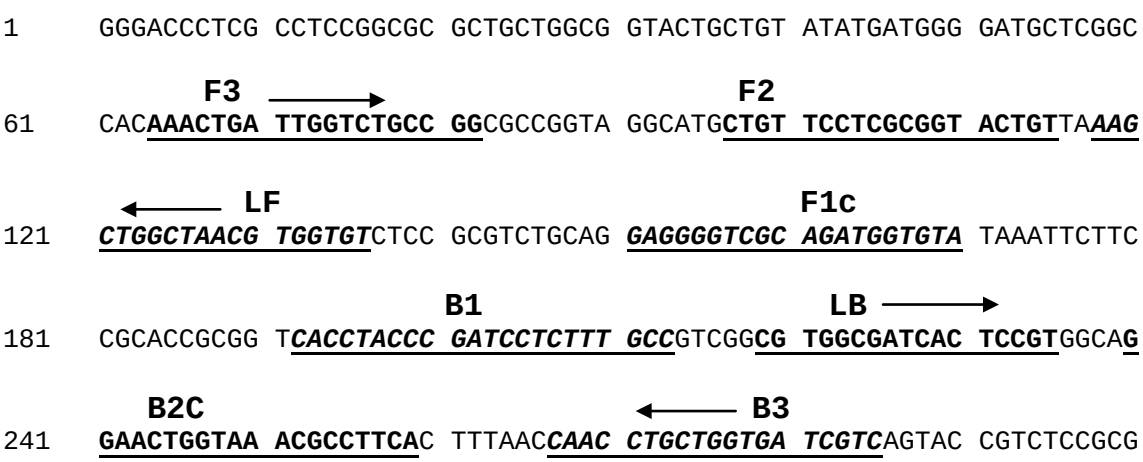

Figure 17. Location of the six LAMP primers, namely the outer primers (F3 and B3) , the inner primers (FIP and BIP) and the labeled loop primers (LF and LB) on the *E. coli malB* (GDB J01648), *E. coli STX-1* (GDB AM230663.1) and *Klebsiella Pneumoniae citw* gene (GDB AF411142) respectively. The forward inner primer (FIP) consists of F1c+ F2 and the backward inner primer consists of B1+B2c. The reverse complimentary sequences of the primers are italicized. For *E. coli mal*B, Loop B and B2 overlap by one base which is depicted between two vertical lines "| A|" and Loop F and F2 are contiguous which are separated by a "*" symbol for ease of reading. The outer primers for *E. coli mal*B are the extended primers which did not form primer dimers in PCR.

LAMP reaction

The LAMP reaction was carried out in a total reaction volume of 25 µL that contained the three primer pairs in the ratio 1:4:8, i.e. 0.2µM each of outer primers (F3 and B3), 0.8µM each of loop primers (LF and LB) and 1.6µM each of inner primers (FIP and BIP) respectively for each organism. For the multiplex reactions, the primers for both *E. coli mal*B and *K. pneumoniae* or *E. coli mal*B and *E. coli STX-1* were mixed in the ratio 1:1 and their individual concentrations were unchanged in the reaction mixture. The other components of the reaction mix were: 2.5 µL of 10X *Bst* DNA polymerase reaction buffer; 1 µL of 8 U/µL *Bst* DNA polymerase (New England Biolabs Inc., MA, USA), 2 µL of 100 mM of $MgSO_4$, 5 µL of Betaine (Sigma Aldrich, MO, USA), 2.5 µL deionized water and 2.5 µL of target sample. The *Bst* DNA polymerase reaction buffer (1X) contained 20mM Tris –HCl (pH 8.8, @ 25ºC), 10mM KCl , 10mM $(NH_2)SO_4$, 2mM $MgSO_4$, 0.1% Triton X-100(New England Biolabs Inc., MA, USA). The LAMP reaction was primarily carried out in a heating block (LAB-LINE, Barnstead International, Dubuque, Iowa, USA). The negative target control (NTC) for LAMP contained all the reagents in the reaction mixture and water (for the target). The LAMP amplification products are detected by several methods, including gel electrophoresis and on lateral flow strips. Shown in **Figure 18** is the detection of LAMP product in a 2% agarose gel with the aid of Sybr DNA staining dye and UV-transillumination.

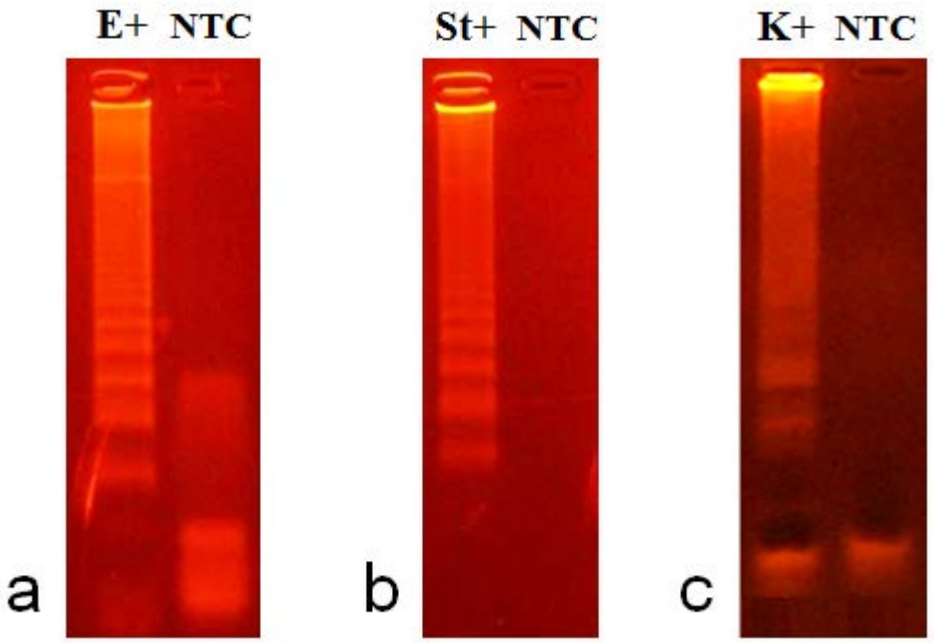

Figure 18. Gel image showing the positive LAMP reaction and its negative target control (NTC) for **a)** *E. coli mal*B **b)** *E. coli STX-1* **c)** *K. pneumoniae*

3.3.4.1 LAMP with labeled primers

As with carrying out PCR with labeled primers, the factors that need to be considered when performing LAMP with labeled primers are that the reaction should remain unaffected by the presence of the labels and that there are sufficient labels to enable a sensitive detection on lateral flow strips. As with PCR the primer-dimer formation during the LAMP reaction needs to be minimized. With six primers present in the reaction mixture, it is a daunting task to prevent the formation of primer-dimers between each of the primers. Also, the length of the inner primers is around 40 nucleotides long which make it difficult to prevent dimers. But, as long as the efficiency of the reaction remains largely unaffected, the dimer formation between the unlabeled primers does not interfere with the detection scheme on the lateral flow strips. It is the dimer formation with the labeled primers which needs to be prevented to eliminate the possibility of a false positive. As LAMP utilizes six primers for amplification, we have the following choices of labeling the primers:

1. Outer primers: The outer primers F3 and B3 can be labeled with FITC and biotin or Dig and biotin.
2. Inner primers: FIP and BIP could be labeled
3. Loop primers: LF and LB could be labeled
4. One of the inner primers + a labeled ssDNA probe

Each of these label choices were first tested for *E. coli mal*B and the most optimum choice was applied to *E. coli STX-1* and *K. pneumoniae*.

1. **Outer primers:**

As the *E. coli mal*B F3 and B3 formed primer dimers when used as the forward and reverse primers in PCR, they were redesigned by extending them on the *E. coli* genome. Their location is as shown in **Figure 17**. From **Figure 15**, it was established earlier that the newly designed extended outer primers do not form a primer dimer as indicated by the flat dissociation curve for the negative target control (NTC). Although the labeled F3 and B3 do not form dimers, the sensitivity of the detection on lateral flow strips after LAMP was found to be poor. When a target which has a copy number of around 10^6 copies/µL was used, a clear distinction between the positive and negative strip can be made (**Figure 19**). When dealing with clinical samples, a target concentration of 10^2 copies/ µL or lesser should be easily detected on the lateral flow strip. But when the target concentration is reduced to below the 10^6 copies/µL limit, the detection on the lateral flow strips becomes inconsistent and therefore unreliable (results not shown). This is primarily because the concentration of the labeled outer primers F3 and B3 in the LAMP reaction is only about 77 nM each. When these are used as the forward and reverse primers in PCR, their concentration is 500 nM in the same reaction volume. Therefore, the choice of labeling the outer primers was disregarded due to poor sensitivity and visual contrast when the target DNA concentration is in the clinically relevant range.

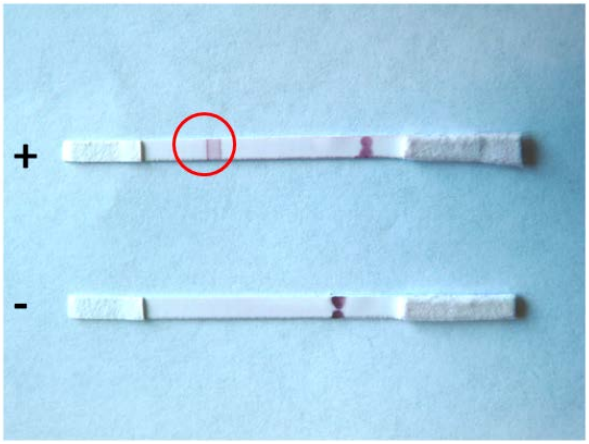

Figure 19. A positive reaction along with its NTC detected on lateral flow strips using labeled outer primers for amplification by LAMP. The concentration of the target is ~3.16 x 10^6 copies/µL as determined by UV spectroscopy at 260 nm.

2. Inner primers:

The labeling of the inner primers FIP with FITC and BIP with biotin for *E. coli mal*B reduced the efficiency and even made the amplification process unreliable. So, although the FIP and BIP primers are present in a large quantity in the reaction mixture, they were not ideal for labeling.

3. Inner primer + ssDNA probe:

In previous studies, a labeled BIP primer has been used in conjunction with a labeled ssDNA probe[93-95] to form the sandwich structure required for detection by lateral flow. This ssDNA probe was added to the reaction mixture after the LAMP reaction was completed and allowed to hybridize with the amplified double stranded DNA with the aid of the strand displacing *Bst* enzyme. This would entail opening of the reaction tube which could possibly lead to contamination of the reaction and of the surroundings by the amplified product. LAMP amplifies with high efficiency with over 10^6 copies in less than an hour. Aerosol from the amplified

product could contaminate the surroundings. Hence this scheme, although successful, was disregarded.

4. Labeled loop primers:

The loop primers are present in sufficient quantity and when labeled do not interfere with the efficiency of the LAMP reaction. Hence they are ideally suited for labeling for detection by lateral flow. As before, the possibility of formation of primer dimers was checked by using real time PCR. Shown in **Figure 20** are the following dissociation curves: the positive control for the reaction (d) and the loop primers added to the PCR reaction without any target for *E. coli mal*B (a), *E. coli STX-1* (b) and *K. pneumoniae* (c) LAMP primers. As seen from the figure, the dissociation curve is flat for the reactions with just the loop primers for the respective organisms showing no presence of primer dimer. A peak at around 81 ^{o}C is seen for the positive control which is representative of the amplified product. Hence the loop primers were chosen to be labeled as they are sensitive, and give rise to no false positives.

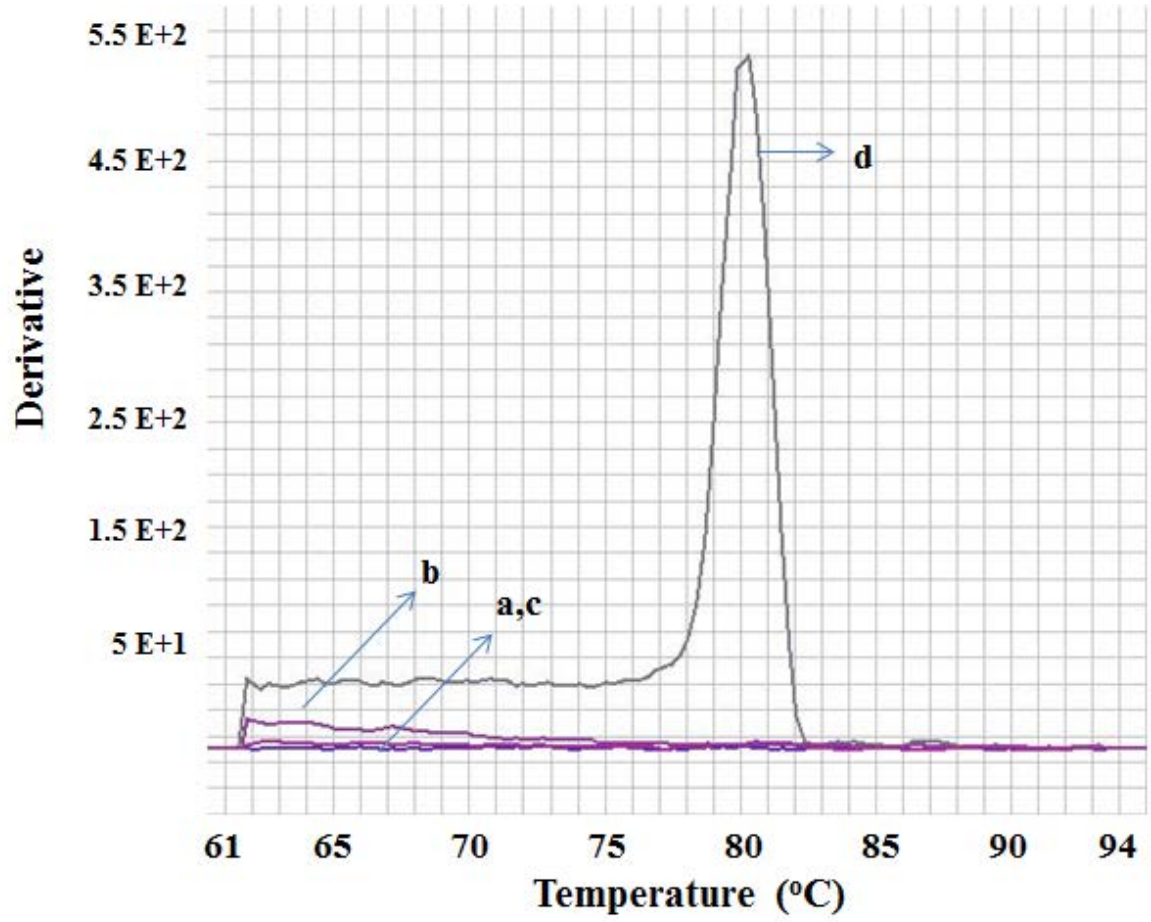

Figure 20. Dissociation curve to check for the presence of primer dimers for the loop primers of **a)** *E. coli mal*B **b)** *E. coli STX-1* and **c)** *K. pneumoniae* along with a **d)** positive control

After the labeled primers, antibody concentrations, nitrocellulose membranes and the pH of the lateral flow buffer have been optimized, the sensitivity of the lateral flow strip detection scheme can be further improved by striping the test line and control line antibodies on the nitrocellulose membrane on a narrow line at a high concentration. This is difficult to achieve with a micropipette or an air brush. In large scale lateral flow strip manufacture, the antibodies are typically sprayed on to the nitrocellulose membrane using lateral flow reagent dispensers which dispense a very fine spray of concentrated antibody solution ensuring the thickness of the test and control line does not exceed 2 mm. Commercially available lateral flow strips, BESt

Type II cassettes (Biohelix Corp, MA, USA) were used to detect the *E. coli mal*B, *E. coli STX-1* and *K. pneumoniae* LAMP products. The BESt type II contains dried colloidal gold nanoparticles (GNPs) conjugated with Anti-Biotin antibody on the conjugate pad and Anti-FITC and Anti-Digoxigenin antibodies striped across the membrane to serve as the test (T) and control (C) lines respectively. The Anti-Digoxigenin immobilized as the control line is actually meant to detect a second set of DNA amplicons labeled with Biotin and Digoxigenin, which in our case is the *E. coli STX-1* and *K. pneumoniae.* After amplification by LAMP, about 10 µL of the product was used as sample for the BESt Type II cassettes and allowed to develop for 5 minutes. **Figure 21** shows the detection of *E. coli mal*B, *E. coli STX-1* and *K. pneumoniae* on lateral flow strips along with their negative target controls.

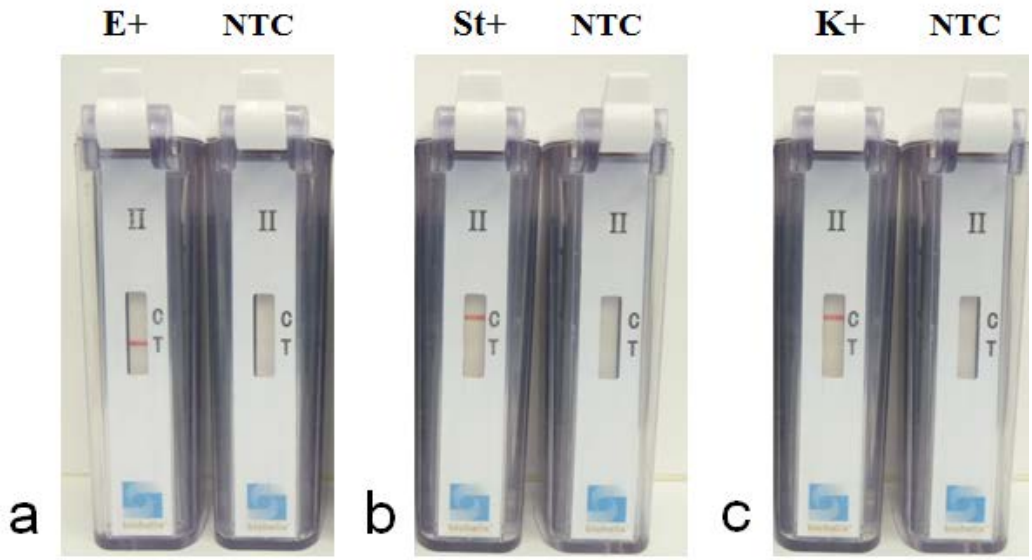

Figure 21. Detection of **a)** *E. coli mal*B (E), **b)** *E. coli STX-1* (ST) and **c)** *K. pneumoniae* on lateral flow strips along with their NTCs.

Specificity of the primers of the LAMP reaction

The specificity of the *E. coli mal*B, *E. coli STX-1*and *K. pneumoniae* primers was checked by performing the LAMP assay for various bacteria namely *Haemophilus influenzae (H),*

*Streptococcus pyogenes (SP), Streptococcus viridans (SV), Corynebacterium diptheriae (C), Nisseria gonorrhea (G), Lactobacillus Iners (L), Staphylococcus epidermis (SE), Klebsiella pneumoniae (K), Escherichia coli mal*B *(E) and E. coli STX-1 (ST).* The LAMP products were seen only when the *E. coli mal*B, *E. coli STX-1* or the *K. pneumoniae* DNA was present in the assay with the matched primer set and was negative for other organisms tested (**Figure 22**). The *E. coli STX-1* DNA was extracted from urine samples which also contains the *E. coli mal*B gene. Hence, when *E. coli mal*B is used as the target with the *E. coli STX-1* primers, there is a ladder showing amplification.

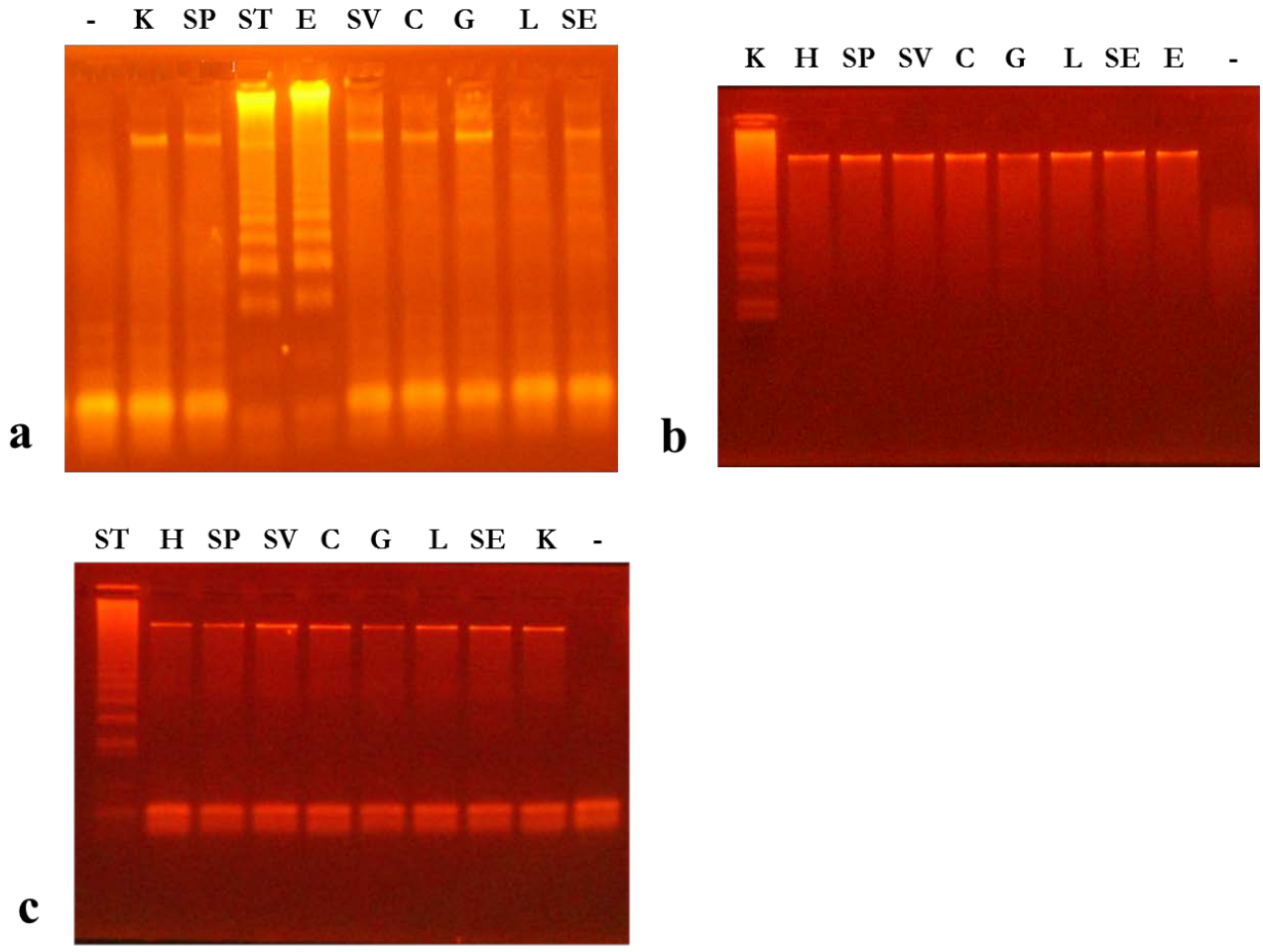

Figure 22. Specificity of the LAMP primers for **a)** *E. coli mal*B, **b)** *K. pneumoniae* and **c)** *E. coli STX-1*

Sensitivity of the LAMP/Lateral flow detection scheme

The sensitivity of the LAMP/lateral flow detection was evaluated only for *E. coli mal*B assay by using a set of serial dilutions of cloned PCR amplicon as the target. The *E. coli mal*B clone was prepared by using StrataClone PCR cloning kit (Stratagene, La Jolla, CA, USA) by incorporating *E. coli mal*B PCR product (307 bps) into the plasmid (~4.3 kbps). The *E. coli* PCR product was prepared by amplifying the genomic DNA with the outer primers F3 and B3 as the forward and reverse primer respectively. The concentration of the *E. coli mal*B clone was determined by UV spectrophotometry (BIO-RAD Smartspec 3000) at 260 nm to be ~$3.14x10^{10}$ copies/µL.

A total of eleven ten-fold serial dilutions of the clone were made, containing ~3 $x10^{10}$copies/µL in 1st dilution to 3 copies/µL in 10th dilution. 11th dilution had less than 3 copies / µL. A volume of 2.5 µL of each of the dilutions was added as target to the LAMP reaction along with a negative target control. A clear ladder pattern is seen for dilutions 1-10 with the intensity of the bands decreasing from dilution #7 (**Figure 23a**). Thus, the sensitivity for an *E. coli mal*B LAMP reaction was determined to be 8 copies/ reaction. Similar results were obtained when the LAMP reaction was performed in an Applied Biosystems 7900HT Real time PCR machine using the 3rd dilution to the 10th dilution as targets (**Figure 23b**). Shown in **Figure 23c** is the detection of the LAMP amplified product on lateral flow strips for the 8th dilution (~$8x10^2$ copies) to the 11th dilution (<3 copies) along with the NTC. The lateral flow strips display excellent sensitivity and are readily able to detect the 10th dilution which contained ~8 copies as the target for LAMP.

A plot of the time taken to cross the threshold value of fluorescence versus the copy number of the *E. coli mal*B clone added as target (**Figure 23d**) shows that when the copy number of the target increases logarithmically, the time taken to reach the threshold fluorescence decreases linearly. Both *E. coli* and *K. pneumoniae* are commonly present in the large intestines

of mammals and an infection is said to have occurred only when the concentration as determined by bacterial culture is greater than 100,000 CFUs/mL of urine. Collection of urine samples from suspected UTI patients is done in a sterile manner so as to avoid contamination of the urine with fecal matter which contains *E. coli*. Even in the worst cases of contamination during collection, the number of cells in CFUs/mL of urine as determined by bacterial culture should not exceed this upper threshold value. Quantification is therefore imperative so as to prevent detection of false positives. Detection by LAMP which has sensitivity of the order of tens of copies could be deemed too sensitive to be used as a reliable quantitative diagnostic tool, but this apparent weakness could be overcome by reducing the duration of amplification so as to detect only those samples with sufficiently high concentration of pathogenic DNA. By reducing the time required for amplification, only those samples with a minimum copy number can be amplified thereby enabling us to set a threshold limit on the copy number which makes it very useful in the clinical setting. If the threshold value for the copy number of *E. coli* is set as 10^2 copies/µL then, performing the LAMP reaction for 50 minutes (**Figure 23d**), amplifies only those targets with copy number greater than this set threshold.

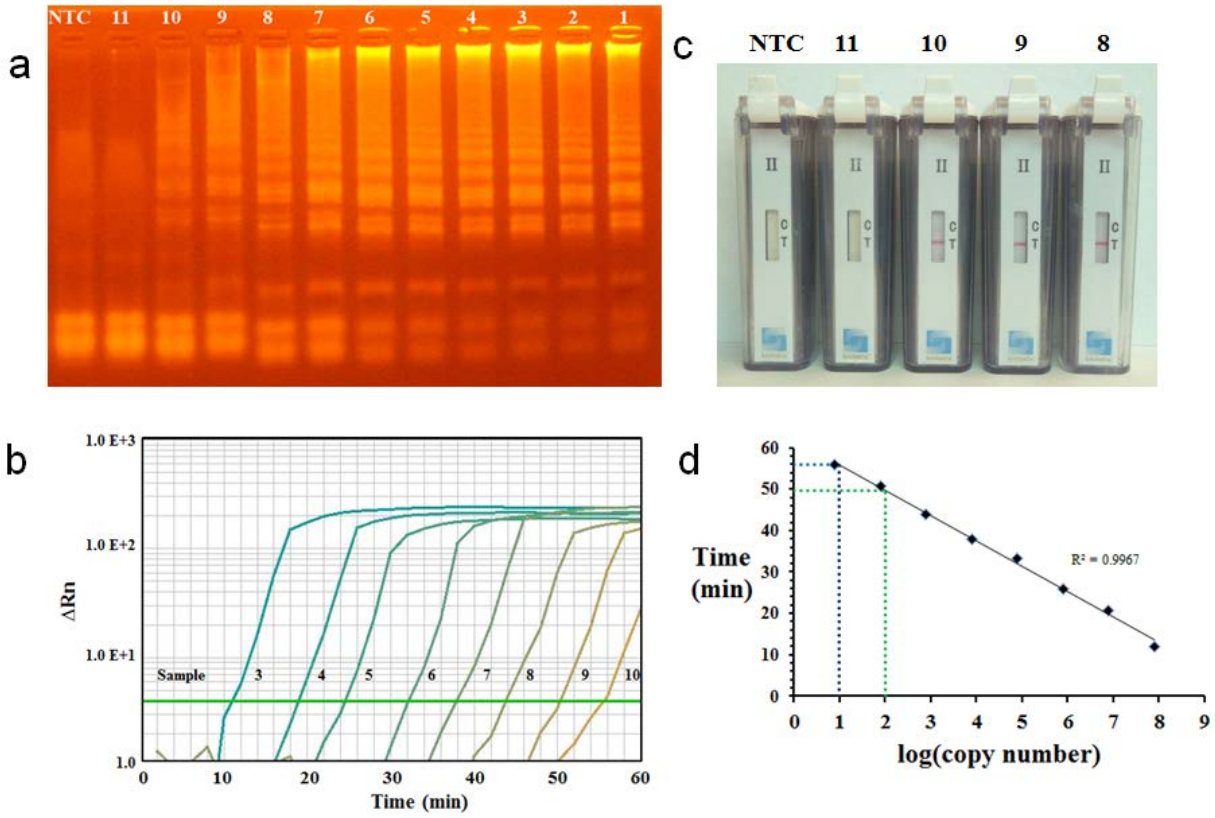

Figure 23. Sensitivity of the LAMP-Lateral flow detection scheme. **a)** Gel image of LAMP reaction performed with serial dilutions of *E. coli malB* clone as target. Lane 1 corresponds to the 1st dilution and lane 11 the 11th dilution. Lane 10 contained ~8 copies which sets the limit for sensitivity. The NTC contains no *E. coli malB* clone. **b)** Real time amplification curves when serial dilutions of *E. coli malB* (Dilutions 3-10) were added as target for LAMP. After the 10th dilution, no amplification was seen. The horizontal green line is fixed as the threshold value of fluorescence. **c)** Detection of 8th to 11th dilution along with the NTC on a commercially available lateral flow strip (BESt Type II cassettes, Biohelix Corp, MA, USA). Dilution 11 and the NTC show no positive test line as expected. **d)** Plot of time taken to reach the threshold value of fluorescence versus log(copy number). The time required for amplification to detect 10 and 100 copies is shown by the blue and green dotted lines respectively.

3.3.4.2 Multiplexing detection

Although an *E. coli* and *K. pneumoniae* infection rarely occurs simultaneously, it is nevertheless advantageous to multiplex their detection. Multiplexing saves time, cost of detection and would be very helpful in administering rapid and accurate treatment to UTI patients. Here, multiplexing relies on sensitive and specific amplification of the target organism's DNA and its subsequent detection on lateral flow strips. Two cases of multiplexing are presented here: The first being the detection of *E. coli* and *K. pneumoniae*, the two most commonly occurring bacteria in UTIs and the second case being the detection of the *E. coli mal*B and *E. coli STX-1* genes in a single reaction and lateral flow strip. The first case is an example of amplification and detection of different bacteria whereas the second case is the further narrowing down of the sub-species of the bacteria. To carry out a successful multiplex LAMP amplification, the primers for both targets need to be present in sufficient quantity and there must be as little cross interaction as possible. In LAMP where there are 6 primers per target, it is obviously very difficult to prevent all primer interactions. Fortunately, as long as the labeled primers do not interact with one another and the efficiency of the amplification for either target remains unaffected, multiplexing can be accomplished in a straight forward manner.

Case 1. *E. coli mal*B + *K. pneumoniae*

The primers are mixed in the ratio 1:1 in a total reaction mixture of 25 µL and their individual concentrations are unchanged i.e. the concentration of *E. coli mal*B primers and the *K. pneumoniae* primers are the same as when the LAMP reaction is carried out individually. The loop primers, LF and LB of *E. coli mal*B are labeled with FITC and Biotin and the LF and LB primers of *K. pneumoniae* are labeled with Dig and Biotin as before (**Table 7**). Earlier, it has been established that there is no formation of dimers between the loop primers of *E. coli mal*B and *K. pneumoniae* when the reactions are performed individually. Now, when multiplexing their amplification, we need to consider the formation of dimers between the labeled loop primers of the two organisms, namely the dimer formation between LF-FITC of *E. coli mal*B and LB-Biotin of *K. pneumoniae*, LF-Dig of *K. pneumoniae* and LB-Biotin of *E. coli mal*B and finally, when all four loop primers are mixed together. Shown in **Figure 24** is the dissociation curve when each of the individual cases mentioned above are checked for the formation of primer-dimers. As seen in the figure, there is no formation of primer-dimers between any of the loop primers of *E. coli mal*B and *K. pneumoniae*. Shown in **Figure 25** is the gel image for the detection of *E. coli mal*B and *K. pneumoniae* for the multiplex reaction and its detection on lateral flow strips respectively.

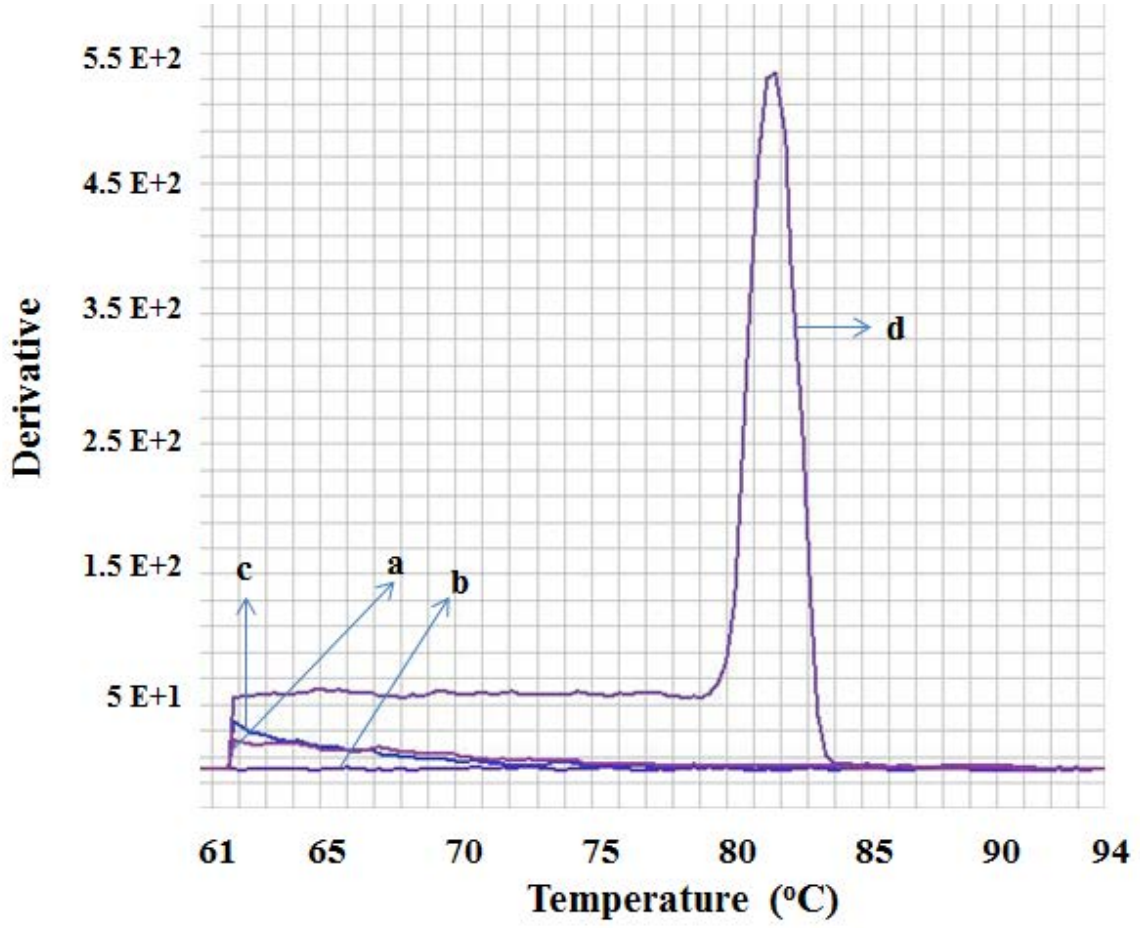

Figure 24. Dissociation curve to check for the presence of primer dimer formation between **a)** LF-FITC of *E. coli mal*B and LB-Biotin of *K. pneumoniae*, **b)** LF-Dig of *K. pneumoniae* and LB-Biotin of *E. coli mal*B and **c)** when all four loop primers are added together. **d)** Positive control for the reaction showing the dissociation temperature for amplified dsDNA to be around 83 ^{o}C.

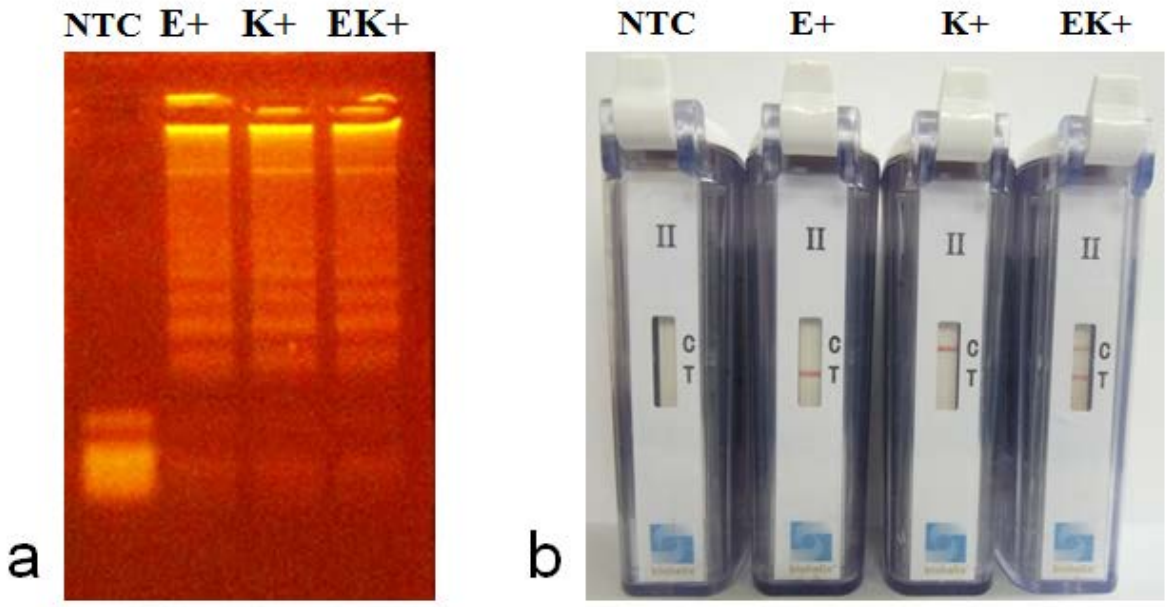

Figure 25. Detection of multiplexed amplification with mixed primers of *E. coli mal*B and *K. pneumoniae* when *E. coli mal*B (E), *K. pneumoniae* (K) and both *E. coli mal*B and *K. pneumoniae* (EK) were added as targets in the LAMP reaction on the **a)** agarose gel **b)** Lateral flow strips

Case 2. *E. coli mal*B + E. coli STX-1

The loop primers, LF and LB of *E. coli mal*B are labeled with FITC and Biotin and the LF and LB primers of *E. coli STX-1* are labeled with Dig and Biotin as before (**Table 7**). The ratio of the primers in the reaction mixture is 1:1 and their individual concentrations are unchanged.

As with the *E. coli mal*B + *K. pneumoniae*, we need to consider the formation of dimers between the labeled loop primers of the two genes, namely the dimer formation between LF-FITC of *E. coli mal*B and LB-Biotin of *E. coli STX-1*, LF-Dig of *E. coli STX-1* and LB-Biotin of *E. coli mal*B and finally, when all four loop primers are mixed together. Shown in **Figure 26** is the dissociation curve when each of the individual cases mentioned above are checked for the formation of primer-dimers. As seen in the figure, there is no formation of primer-dimers between any of the loop primers of *E. coli mal*B and *E. coli STX-1*. The target for the multiplex reaction is the DNA extracted from urine samples, which contain both the *mal*B and the STX-1 genes in the same target dsDNA. Shown in **Figure 27** is the gel image for the detection of *E. coli mal*B and *E. coli STX-1* for the multiplex reaction and its detection on lateral flow strips respectively.

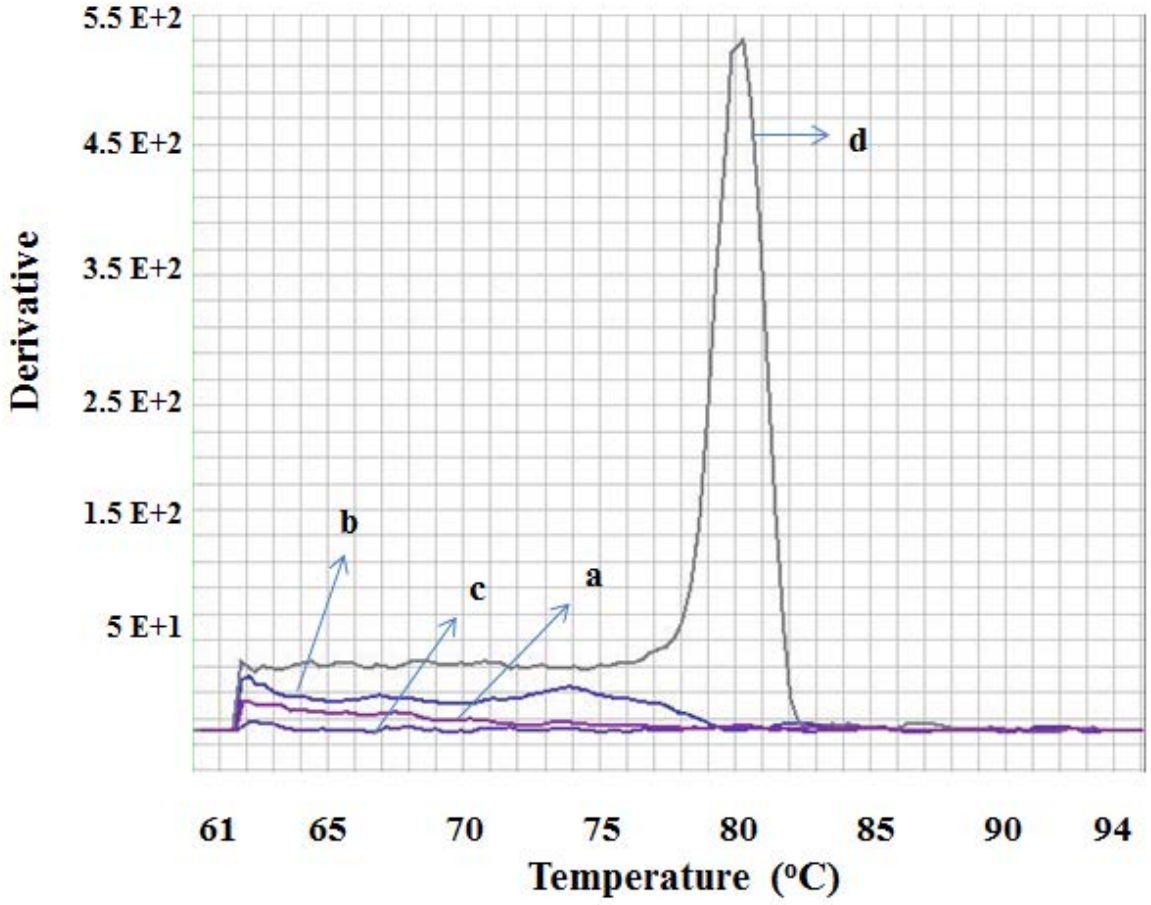

Figure 26. Dissociation curve to check for the presence of primer dimer formation between **a)** LF-FITC of *E. coli mal*B and LB-Biotin of *E. coli STX-1*, **b)** LF-Dig of *E. coli STX-1* and LB-Biotin of *E. coli mal*B and **c)** when all four loop primers are added together. **d)** Positive control for the reaction showing the dissociation temperature for amplified dsDNA to be around 80 ^{o}C.

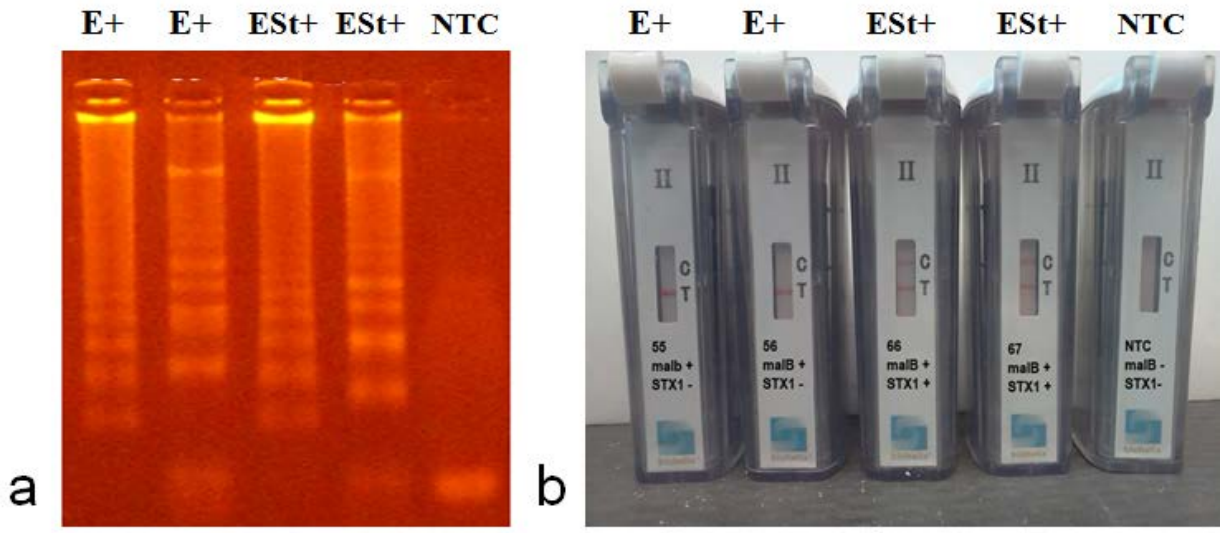

Figure 27. Detection of multiplexed amplification with mixed primers of *E. coli mal*B and *E. coli STX-1* when *E. coli mal*B (E), *E. coli STX-1* (St) and both *E. coli mal*B and *E. coli STX-1* (ESt) were added as targets in the LAMP reaction on the **a)** agarose gel **b)** Lateral flow strips.

3.3.4.3 Lamp-lateral flow detection of clinical samples

The bacterial strains used in the study were obtained from the microbiology laboratories of the Children's Hospital of Pittsburgh. The urine samples used in this study were residual samples that were sent to the microbiology laboratories from patients with suspected UTI and were available after all the clinically required studies (i.e. culture and sensitivity) were performed. The samples were anonymized by a "honest broker". These studies were approved as exempt by the IRB of University of Pittsburgh. DNA was extracted from bacterial and urine samples using QIAamp DNA Mini-Kit (Qiagen, CA, USA).

96 fresh urine samples from patients with suspected UTI were obtained from the microbiology laboratories of Children's Hospital of Pittsburgh. DNA was extracted from these urine samples using QIAamp DNA Mini-Kit (Qiagen, CA, USA) and this was used as the target for PCR with the outer primers F3 and B3 as the forward and reverse primers respectively for both *E. coli mal*B and *K. pneumoniae*. As the LAMP reaction performs well in biological samples without too much sample preprocessing [91,92], 5 µL of unprocessed urine was used directly as target for the LAMP reaction (total 25uL) for both *E. coli mal*B and *K. pneumoniae* and the results were compared to both PCR and bacterial culture results. The reactions were performed individually for *E. coli mal*B and *K. pneumoniae* and also multiplexed by mixing the primers in 1:1 ratio as described before. The results from the bacterial culture was taken as positive when there are greater than 100,000 CFUs/ml. Out of the 96 urine samples, 9 were positive for *E. coli mal*B by bacterial culture, whereas 8 were positive by both PCR with extracted DNA and LAMP with direct urine as target using the *E. coli mal*B LAMP primers. 87 samples were negative for *E. coli mal*B by bacterial culture and 88 were negative for both PCR

and LAMP. Furthermore, the 8 samples which were positive by LAMP amplification were also positive by the lateral flow assay. For *K. pneumoniae*, out of the 96 samples, 3 were positive by bacterial culture and PCR with extracted DNA and all these were positive by LAMP/lateral flow with direct urine as target. The results are summarized in **Table 8** and **Table 9**. The sensitivity and specificity of the multiplex reactions for *E. coli mal*B and *K. pneumoniae* are summarized in **Table 10**. The possible reason for the mismatch of one of the bacterial culture results with PCR and LAMP for *E. coli mal*B could be due to excessive degradation of the *E. coli* DNA in the urine sample.

E. coli STX-1 is typically found in stool and was therefore not screened for in the 96 urine samples. For *E. coli STX-1*, culture plates which were positive for *E. coli STX-1* were used. The cells were cultured overnight at 37 ^{o}C and then the DNA was extracted from them. PCR was run with both the *E. coli mal*B primers and *E. coli STX-1* primers. Out of the 20 culture samples, all were positive for *E. coli mal*B and 11 were positive for *E. coli STX-1* by PCR. LAMP was conducted with only the *E. coli STX-1* primers (individual reaction) and also multiplexed with *E. coli mal*B and *E. coli STX-1* primers mixed in the ratio 1:1. 11 out of 11 samples positive by PCR and bacterial culture were positive by both LAMP-lateral flow. The results are summarized in **Table 8** and **Table 9**. The sensitivity and specificity of the multiplex reactions for *E. coli mal*B, *K. pneumoniae* and *E. coli STX-1* are summarized in **Table 10**.

Table 8. Comparison of LAMP-Lateral flow detection for both *E. coli mal*B and *K. pneumoniae* versus PCR and bacterial culture methods from urine samples with patients suspected with UTI. The PCR and LAMP-Lateral flow results for *E. coli STX-1* are for extracted DNA from culture plates.

	PCR			LAMP-Lateral flow			Bacterial culture		
	malB	*STX-1*	*Kleb*	*malB*	*STX-1*	*Kleb*	*malB*	*STX-1*	*Kleb*
Number positive	8	11	3	8	11	3	9	11	3
Number negative	88	9	93	88	9	93	87	9	93

Table 9. Sensitivity and specificity for LAMP-Lateral flow detection as compared to PCR and cell culture methods.

	*E. coli mal*B		*E. coli STX-1*		*K. pneumoniae*	
	Vs PCR	Vs Bacterial culture	Vs PCR	Vs Bacterial culture	Vs PCR	Vs Bacterial culture
Sensitivity	100%	89%	100%	100%	100%	100%
Specificity	100%	100%	100%	100%	100%	100%

Table 10. Sensitivity and specificity as compared to individual LAMP reactions and PCR of *E. coli mal*B, *K. pneumoniae* and *E. coli STX-1* when multiplex primer set is used.

Primer set	*E. coli mal*B + *K. pneumoniae*	*E. coli mal*B + *E. coli STX-1*	
	Vs Individual LAMP reaction	Vs Individual LAMP reaction	Vs PCR
Sensitivity for *E. coli mal*B	100%	100%	100%
Specificity for *E. coli mal*B	100%	100%	100%
Sensitivity for *K. pneumoniae*	100%	NA	100%
Specificity for *K. pneumoniae*	100%	NA	100%
Sensitivity for *E. coli STX-1*	NA	100%	100%
Specificity for *E. coli STX-1*	NA	100%	100%

3.4 DISCUSSION

As detailed before, DNA amplification by LAMP combined with lateral flow detection serves as an extremely sensitive and specific DNA detection strategy which is well suited for the clinical setting. The ability to carry out the reaction for shorter intervals of time to place an upper threshold limit on the detection could aid in replacing the cumbersome cell culture techniques, or in the least restrict them to only those samples which have been screened by LAMP-Lateral flow detection. The use of colloidal gold as reporter particles in lateral flow assays is at best qualitative, but when used in conjunction with a sensitive and specific LAMP assay provides a reliable detection scheme which is quantitative. Detection on lateral flow strips is rapid (~5 minutes) and the results can be viewed visually without the need for any instrumentation. Moreover, lateral flow strips can be mass produced at a very low cost and can be stored in ambient conditions without too much loss in sensitivity.

Fortuitously the *Bst* DNA polymerase is not inhibited by the urea present in urine when compared to *Taq* DNA polymerase, enabling direct patient urine containing *E. coli* and *K. pneumoniae* cells to be used as target for LAMP amplification. Urine samples with a concentration of greater than 100,000 CFUs/mL of urine, determined by bacterial culture methods are easily picked up by LAMP, whereas for samples with a concentration less than this threshold value are not amplified when performed without DNA extraction. This reduces sample handling to a minimum and thus could pave the way for integrated point-of-care devices where the reaction and detection takes place in a closed system to give a qualitative ‘yes’ or ‘no’ answer in less than an hour. We report here a cost effective and rapid diagnosis method to detect

*E. coli mal*B, *E. coli STX-1* and *K. pneumoniae* in human urine. Multiplexing the amplification by LAMP for the detection of two organisms has also been achieved which not only saves cost of reagents, but also time for detection is reduced. The total cost of the reagents for the LAMP reaction and its subsequent detection on lateral flow strips when mass produced does not exceed a dollar. The isothermal requirements of LAMP, high specificity, minimal sample preprocessing coupled with the sensitivity of the lateral flow detection makes this detection scheme very promising for point-of-care diagnostic applications in developing countries.

4.0 SUMMARY AND FUTURE OUTLOOK

DNA-based biosensors have tremendous potential to be used in point-of-care diagnostics primarily due to their unparalled specificity and the ease of fabricating sensor substrates with DNA molecules. DNA molecules can be immobilized onto substrates such as glass, gold, silicon, carbon, etc. by using chemistry which is well known. The use of thiolated DNA which self-assemble or through functional alkanethiol monolayers on gold, biotinylated DNA strands on avidin coated surfaces, carbodiimde chemistry for carbon surfaces, physical adsorption, etc. are some of the more commonly used immobilization techniques. Unlike proteins, DNA molecules are more robust and the sensor surface can be regenerated easily by chemically or thermally induced dehybridization.

Typically, DNA biosensors are based on the recognition of the hybridization of a complementary strand or the detection of an amplified DNA product. The hybridization event must produce a noticeable change either through an appropriate indicator or by monitoring other changes brought about by the duplex formation. The conditions for solution hybridization such as temperature, ionic strength, presence of accelerators, etc. have to be optimized. DNA hybridization events can be detected using optical, electrochemical, piezoelectric or colorimetric methods as detailed in Chapter 1 (Pg 4). Label free methods are more sought after as it reduces the complexity of adding the label to the target strand which needs to be detected. DNA microarrays which have revolutionized the genetic analysis can perform rapid multiplex DNA hybridization assays with high precision which is of immense value in the detection of genetic mutations, infectious diseases, gene expression and forensics. Single strand DNA is imprinted at

a high density on these “chips” which are then scanned by a laser for the detection of hybridization events. Hundreds of different sequences can be analyzed at a given time giving great flexibility and reducing time. However, all these commercial devices which utilize DNA hybridization either require labels or are generally too expensive to be used as point-of-care sensors. In this work, we propose an alternative route to the conventional DNA hybridization by successfully detecting DNA mutations by examining the viscoelastic properties of ssDNA strands and secondly, by using a rapid, isothermal DNA amplification scheme coupled with detection of the amplified product on low cost lateral flow strips.

In the first part of this work, the ssDNA’s ability to form sequence dependent unique 3-D conformation in solution is utilized to distinguish between the wild and mutant type DNA. We have shown that when the wild type ssDNA strands are immobilized onto a substrate to form a ssDNA film, the film’s viscoelastic properties are different from that of the mutant type ssDNA film. The *p53* gene was used as a case study and appreciable differences in the *p53* wild type ssDNA film and *p53* R type mutant ssDNA film were observed. The differences between the wild type and mutant type ssDNA films can be maximized by including different fragments of the gene which contain the mutation and technically, there is no upper limit on the number of bases that can be screened. The sensitivity can be further improved by using MEMS/NEMS devices operating in the resonant mode, where extremely high frequencies in the GHz range and high Q-factors can be obtained. This would greatly increase sensitivity, reduce power consumption and importantly make it possible to screen multiple samples in a cost effective manner. This low cost, rapid, label free mutation screening technique therefore has great promise.

In the second part of this work, a simpler, more cost effective route to detect infectious organisms for point-of-care diagnostics is proposed. Timely point-of-care diagnosis for life threatening infectious diseases is of paramount importance. The strategy is to isothermally

amplify the DNA with labels and then detecting the labels (haptens) via hapten-antibody binding which is faster and more efficient than DNA hybridization. Isothermal amplification by LAMP does away with expensive thermal cyclers required for PCR and does not require the use of skilled personnel which is ideally suited for point-of-care applications. Also, another distinct advantage of LAMP over PCR is that minimal sample preprocessing is required. We have shown that direct patient urine samples can be readily used without inhibiting the *Bst* strand displacing enzyme which greatly simplifies the detection scheme. With careful design of labeled DNA primers multiplexing detection of two organisms is possible and the sensitivity and specificity of the detection of the amplified product on lateral flow strips is comparable to PCR and bacterial culture methods. Detection on lateral flow strips is attractive as the strips are cheap to manufacture, do not require instrumentation to read it and amount of DNA present after LAMP amplification (~10^6 copies) is sufficient to ensure a high sensitive and specific detection. In future, we envision an integrated and self-contained point-of-care device where after the addition of the patient sample into the device, the results are viewed on the lateral flow strip and disposed off. The LAMP reaction mixture with the reagents and the enzyme is stable at room temperature for 20 days and does not require refrigeration. Integrating a chemical heater which maintains around 63 – 65 ^{o}C with such a device would require no electricity at all to carry out the detection. Therefore, considering all the above factors, the LAMP-lateral flow detection scheme thus has immense potential to be deployed as a reliable point-of-care diagnostic tool.

BIBLIOGRAPHY

(1) Byfield, M. P.; Abuknesha, R. A. *Biosensors and Bioelectronics* **1994**, *9*, 373.

(2) Marazuela, M.; Moreno-Bondi, M. *Analytical and Bioanalytical Chemistry* **2002**, *372*, 664.

(3) Newman, J. D.; Turner, A. P. F. *Biosensors and Bioelectronics* **2005**, *20*, 2435.

(4) Yoo, E.-H.; Lee, S.-Y. *Sensors* **2010**, *10*, 4558.

(5) ZHANG, G.; ZHOU, Y.; YUAN, J.; REN, S. *A chemiluminescence fiber-optic biosensor for detection of DNA hybridization*; Taylor & Francis: Philadelphia, PA, ETATS-UNIS, 1999; Vol. 32.

(6) Kleinjung, F. *Analytica Chimica Acta* **1997**, *350*, 51.

(7) Uddin, A. H.; Piunno, P. A.; Hudson, R. H.; Damha, M. J.; Krull, U. J. *Nucleic Acids Research* **1997**, *25*, 4139.

(8) Piunno, P.; Krull, U.; Hudson, R.; Damha, M.; Cohen, H. *Analytical Chemistry* **1995**, *67*, 2635.

(9) Abel, A. P.; Weller, M. G.; Duveneck, G. L.; Ehrat, M.; Widmer, H. M. *Analytical Chemistry* **1996**, *68*, 2905.

(10) Graham, C. R.; Leslie, D.; Squirrell, D. J. *Biosensors and Bioelectronics* **1992**, *7*, 487.

(11) Ferguson, J.; Boles, C.; Adams, C.; Walt, D. *Nature Biotechnology* **1996**, *14*, 1681.

(12) Walt, D. R. *Science (New York, N.Y.)* **2000**, *287*, 451.

(13) Lee, M.; Walt, D. R. *Analytical Biochemistry* **2000**, *282*, 142.

(14) Millan, K. M.; Mikkelsen, S. R. *Analytical Chemistry* **1993**, *65*, 2317.

(15) Campbell, C.; Gal, D.; Cristler, N.; Banditrat, C.; Heller, A. *Analytical Chemistry* **2002**, *74*, 158.

(16) Evtugyn, G. *Analytica Chimica Acta* **2003**, *479*, 125.

(17) Patolsky, F.; Weizmann, Y.; Willner, I. *Journal of the American Chemical Society* **2002**, *124*, 770.

(18) Kerman, K.; Kobayashi, M.; Tamiya, E. *Measurement Science and Technology* **2004**, *15*, R1.

(19) Arora, K.; Chaubey, A.; Singhal, R.; Singh, R.; Pandey, M.; Samanta, S.; Malhotra, B.; Chand, S. *Biosensors and Bioelectronics* **2006**, *21*, 1777.

(20) dos Santos Riccardi, C.; Yamanaka, H.; Josowicz, M.; Kowalik, J.; Mizaikoff, B.; Kranz, C. *Analytical Chemistry* **2006**, *78*, 1139.

(21) Kerman, K. *Electrochemistry Communications* **2003**, *5*, 887.

(22) Wang, J.; Kawde, A. N.; Sahlin, E. *The Analyst* **2000**, *125*, 5.

(23) Arora, K.; Prabhakar, N.; Chand, S.; Malhotra, B. D. *Biosensors & Bioelectronics* **2007**, *23*, 613.

(24) Sauerbrey, G. *Zeitschrift für Physik* **1959**, *155*, 206.

(25) Lazerges, M.; Perrot, H.; Antoine, E.; Defontaine, A.; Compere, C. *Biosensors and Bioelectronics* **2006**, *21*, 1355.

(26) Ye, J.; Letcher, S. V.; Rand, A. G. *Journal of Food Science* **1997**, *62*, 1067.

(27) Towery, R. B.; Fawcett, N. C.; Zhang, P.; Evans, J. A. *Biosensors & Bioelectronics* **2001**, *16*, 1.

(28) Su, X.; Robelek, R.; Wu, Y.; Wang, G.; Knoll, W. *Analytical Chemistry* **2004**, *76*, 489.

(29) Larsson, C.; Rodahl, M.; Hook, F. *Analytical Chemistry* **2003**, *75*, 5080.

(30) Sato, K.; Hosokawa, K.; Maeda, M. *Analytical sciences : the international journal of the Japan Society for Analytical Chemistry* **2007**, *23*, 17.

(31) Teles, F.; Fonseca, L. *Talanta* **2008**, *77*, 606.

(32) Hestekin, C. N.; Barron, A. E. *Electrophoresis* **2006**, *27*, 3805.

(33) Kwok, P. Y. *Annual review of genomics and human genetics* **2001**, *2*, 235.

(34) Cotton, R. G. *Mutation research* **1993**, *285*, 125.

(35) Orita, M.; Suzuki, Y.; Sekiya, T.; Hayashi, K. *Genomics* **1989**, *5*, 874.

(36) Hayashi, K.; Yandell, D. *Human Mutation* **1993**, *2*, 338.

(37) Balogh, K.; Patocs, A.; Majnik, J.; Racz, K.; Hunyady, L. *Molecular Genetics and Metabolism* **2004**, *83*, 74.

(38) Muyzer, G.; Smalla, K. *Antonie van Leeuwenhoek* **1998**, *73*, 127.

(39) Larsen, L. A.; Christiansen, M.; Vuust, J.; Andersen, P. S. *Human Mutation* **1999**, *13*, 318.

(40) Tabone, T. *Hum. Mutat.* **2008**, *29*, 886.

(41) Hollstein, M.; Sidransky, D.; Vogelstein, B.; Harris, C. C. *Science (New York, N.Y.)* **1991**, *253*, 49.

(42) Rodahl, M.; Kasemo, B. *Sensors and Actuators A: Physical* **1996**, *54*, 448.

(43) Su, X.; Wu, Y.-J.; Robelek, R.; Knoll, W. *Langmuir* **2005**, *21*, 348.

(44) Aung, K. M. M.; Ho, X.; Su, X. *Sensors and Actuators B: Chemical* **2008**, *131*, 371.

(45) Behling, C.; Lucklum, R.; Hauptmann, P. *Ultrasonics, Ferroelectrics and Frequency Control, IEEE Transactions on* **1999**, *46*, 1431.

(46) Lucklum, R.; Behling, C.; Cernosek, R.; Martin, S. *Journal of Physics D: Applied Physics* **1997**, *30*, 346.

(47) Lucklum, R.; Hauptmann, P. "Thin film shear modulus determination with quartz crystal resonators: a review"; Frequency Control Symposium and PDA Exhibition, 2001. Proceedings of the 2001 IEEE International, 2001.

(48) Voinova, M. V.; Rodahl, M.; Jonson, M.; Kasemo, B. *Physica Scripta* **1999**, *59*, 391.

(49) Reed, C. E.; Kanazawa, K.; Kaufman, J. H. *Journal of Applied Physics* **1990**, *68*, 1993.

(50) Su, X.; Wu, Y.; Knoll, W. *Biosensors and Bioelectronics* **2005**, *21*, 719.

(51) Lucarelli, F.; Tombelli, S.; Minunni, M.; Marrazza, G.; Mascini, M. *Analytica Chimica Acta* **2008**, *609*, 139.

(52) Hook, F.; Ray, A.; Norden, B.; Kasemo, B. *Langmuir* **2001**, *17*, 8305.

(53) Cho, Y. *Journal of Colloid and Interface Science* **2004**, *278*, 44.

(54) D'Orazio, P. *Clinica Chimica Acta* **2003**, *334*, 41.

(55) Marco, M. P.; Gee, S.; Hammock, B. D. *Trac-Trends in Analytical Chemistry* **1995**, *14*, 341.

(56) Rogers, K. R. *Molecular Biotechnology* **2000**, *14*, 109.

(57) Vijayendran, R. A.; Leckband, D. E. *Analytical Chemistry* **2001**, *73*, 471.

(58) Davies, D. R.; Padlan, E. A.; Sheriff, S. *Annual Review of Biochemistry* **1990**, *59*, 439.

(59) Butler, J. E.; Ni, L.; Brown, W. R.; Joshi, K. S.; Chang, J.; Rosenberg, B.; Voss, J. E. W. *Molecular Immunology* **1993**, *30*, 1165.

(60) Butler, J. E.; Ni, L.; Nessler, R.; Joshi, K. S.; Suter, M.; Rosenberg, B.; Chang, J.; Brown, W. R.; Cantarero, L. A. *Journal of Immunological Methods* **1992**, *150*, 77.

(61) Shriver-Lake, L. C.; Donner, B.; Edelstein, R.; Breslin, K.; Bhatia, S. K.; Ligler, F. S. *Biosensors & Bioelectronics* **1997**, *12*, 1101.

(62) Bhatia, S. K.; Shriverlake, L. C.; Prior, K. J.; Georger, J. H.; Calvert, J. M.; Bredehorst, R.; Ligler, F. S. *Analytical Biochemistry* **1989**, *178*, 408.

(63) Aizawa, H.; Gokita, Y.; Park, J. W.; Yoshimi, Y.; Kurosawa, S. *Ieee Sensors Journal* **2006**, *6*, 1052.

(64) Caruso, F.; Rodda, E.; Furlong, D. N. *Journal of Colloid and Interface Science* **1996**, *178*, 104.

(65) Narang, U.; Anderson, G. P.; Ligler, F. S.; Burans, J. *Biosensors and Bioelectronics* **1997**, *12*, 937.

(66) Turková, J. *Journal of Chromatography B: Biomedical Sciences and Applications* **1999**, *722*, 11.

(67) Peluso, P.; Wilson, D. S.; Do, D.; Tran, H.; Venkatasubbaiah, M.; Quincy, D.; Heidecker, B.; Poindexter, K.; Tolani, N.; Phelan, M.; Witte, K.; Jung, L. S.; Wagner, P.; Nock, S. *Analytical Biochemistry* **2003**, *312*, 113.

(68) Danczyk, R.; Krieder, B.; North, A.; Webster, T.; HogenEsch, H.; Rundell, A. *Biotechnology and Bioengineering* **2003**, *84*, 215.

(69) Vashist, S. K.; Raiteri, R.; Tewari, R.; Bajpai, R. P.; Bharadwaj, L. M. *Journal of Physics: Conference Series* **2006**, *34*, 806.

(70) Karlsson, R.; Fält, A. *Journal of Immunological Methods* **1997**, *200*, 121.

(71) Babacan, S.; Pivarnik, P.; Letcher, S.; Rand, A. G. *Biosensors and Bioelectronics* **2000**, *15*, 615.

(72) Rusmini, F.; Zhong, Z.; Feijen, J. *Biomacromolecules* **2007**, *8*, 1775.

(73) Lu, B.; Smyth, M. R.; O'Kennedy, R. *The Analyst* **1996**, *121*, 29R.

(74) Su, X.; Wu, Y.-J.; Robelek, R.; Knoll, W. *Langmuir* **2004**, *21*, 348.

(75) Janshoff, A.; Galla, H.-J.; Steinem, C. *Angewandte Chemie International Edition* **2000**, *39*, 4004.

(76) Rabbany, S. Y.; Piervincenzi, R.; Judd, L.; Kusterbeck, A. W.; Bredehorst, R.; Hakansson, K.; Ligler, F. S. *Analytical Chemistry* **1997**, *69*, 175.

(77) Selinger, J. V.; Rabbany, S. Y. *Analytical Chemistry* **1997**, *69*, 170.

(78) Michael J.G, F. *Best Practice & Research Clinical Gastroenterology* **2004**, *18*, 233.

(79) Russo, T. A.; Johnson, J. R. *Microbes and Infection* **2003**, *5*, 449.

(80) Marrs, C. F.; Zhang, L.; Foxman, B. *FEMS Microbiology Letters* **2005**, *252*, 183.

(81) Leung, A. K. C.; Robson, W. L. M.; Davies, H. D. *Advances in Therapy* **2006**, *23*, 519.

(82) Clarke, S. C. *Diagnostic Microbiology and Infectious Disease* **2001**, *41*, 93.

(83) Sato, Y. *Nippon rinsho. Japanese journal of clinical medicine* **2002**, *60*, 2210.

(84) Bonacorsi, S.; Bingen, E. *International Journal of Medical Microbiology* **2005**, *295*, 373.

(85) Paton, A. W.; Paton, J. C. *Journal of Clinical Microbiology* **1998**, *36*, 598.

(86) Karmali, M. A. *Clinical Microbiology Reviews* **1989**, *2*, 15.

(87) Podschun, R.; Ullmann, U. *Clin. Microbiol. Rev.* **1998**, *11*, 589.

(88) Jarvis, W. R.; Munn, V. P.; Highsmith, A. K.; Culver, D. H.; Hughes, J. M. *Infection Control* **1985**, *6*, 68.

(89) Notomi, T.; Okayama, H.; Masubuchi, H.; Yonekawa, T.; Watanabe, K.; Amino, N.; Hase, T. *Nucleic Acids Research* **2000**, *28*, e63.

(90) Nagamine, K. *Molecular and Cellular Probes* **2002**, *16*, 223.

(91) Hill, J.; Beriwal, S.; Chandra, I.; Paul, V.; Kapil, A.; Singh, T.; Wadowsky, R.; Singh, V.; Goyal, A.; Jahnukainen, T.; Johnson, J.; Tarr, P.; Vats, A. *Journal of Clinical Microbiology* **2008**, *46*, 2800.

(92) Mori, Y. *Biochemical and Biophysical Research Communications* **2001**, *289*, 150.

(93) Kiatpathomchai, W.; Jaroenram, W.; Arunrut, N.; Jitrapakdee, S.; Flegel, T. *Journal of Virological Methods* **2008**, *153*, 214.

(94) Nimitphak, T.; Kiatpathomchai, W.; Flegel, T. *Journal of Virological Methods* **2008**, *154*, 56.

(95) Njiru, Z.; Ouma, J.; Enyaru, J.; Dargantes, A. *Experimental parasitology* **2010**, *125*, 196.

(96) James, H.; Ebert, K.; McGonigle, R.; Reid, S.; Boonham, N.; Tomlinson, J.; Hutchings, G.; Denyer, M.; Oura, C.; Dukes, J. *Journal of Virological Methods* **2010**, *164*, 68.

(97) Brooks, D.; Devine, D.; Harris, P.; Harris, J.; Miller, M.; Olal, A.; Spiller, L.; Xie, Z. *Clin Chem* **1999**, *45*, 1676.

(98) Lönnberg, M.; Carlsson, J. *Analytical Biochemistry* **2001**, *293*, 224.

(99) van Amerongen, A.; Wichers, J. H.; Berendsen, L. B.; Timmermans, A. J.; Keizer, G. D.; van Doorn, A. W.; Bantjes, A.; van Gelder, W. M. *Journal of biotechnology* **1993**, *30*, 185.

(100) Baeumner, A.; Schlesinger, N.; Slutzki, N.; Romano, J.; Lee, E.; Montagna, R. *Analytical Chemistry* **2002**, *74*, 1442.

(101) Zaytseva, N.; Montagna, R.; Lee, E. M.; Baeumner, A. *Analytical and Bioanalytical Chemistry* **2004**, *380*, 46.

(102) Corstjens, P.; Zuiderwijk, M.; Brink, A.; Li, S.; Feindt, H.; Niedbala, S.; Tanke, H. *Clin Chem* **2001**, *47*, 1885.

(103) Pappas, M.; Hajkowski, R.; Hockmeyer, W. *Journal of Immunological Methods* **1983**, *64*, 205.

(104) Ferrie, R. M.; Schwarz, M. J.; Robertson, N. H.; Vaudin, S.; Super, M.; Malone, G.; Little, S. *American Journal of Human Genetics* **1992**, *51*, 251.